PARAMETRIC ANALYSIS AND OPTIMIZATION OF LONG-RANGE BATTERY ELECTRIC VEHICLE THERMAL MANAGEMENT SYSTEMS

by

Tyler Shelly

A Thesis

Submitted to the Faculty of Purdue University

In Partial Fulfillment of the Requirements for the degree of

Master of Science in Mechanical Engineering

School of Mechanical Engineering

West Lafayette, Indiana

December 2020

THE PURDUE UNIVERSITY GRADUATE SCHOOL
STATEMENT OF COMMITTEE APPROVAL

Dr. Justin Weibel, Co-Chair

School of Mechanical Engineering

Dr. Eckhard Groll, Co-Chair

School of Mechanical Engineering

Dr. Davide Ziviani

School of Mechanical Engineering

Approved by:

Dr. Nicole Key

Dedicated to everyone who has been with me and kept me alive through my 25 years. My parents and my good friends Will Arrowood, Jamie Penese, Muzamil Pabani, Chi Young Moon, Dwight and Janet Regier, Adam, and Jordan Schroeder.

ACKNOWLEDGMENTS

I remember when I made the decision to come to Purdue. It was the day I was leaving Kansas to come visit for a tour of the lab I would be working in. That feeling of getting on a plane and going to somewhere new was an incredible feeling. Like I was finally pulling up roots that I did not even know were there. When I finally enrolled, I felt something was missing. When I started classes at Purdue the branding of "150 years of giant leaps" was everywhere, on the buses, the napkins, and the grocery bag they gave me at orientation. Gradually over the course of a few months I began to realize that I was still stuck in Kansas. My body and emotions had made the car ride, but my self-image still had not made the jump. Almost like I was not living authentically. Like I had left because it would allow me to live the life I wanted, but when I arrived, I didn't even know how to start. I had never really done it in the first place. I struggled, and am still struggling, to find my ideal self. It created a sort of paradox for me, I needed to take make a leap but hadn't learned how to jump. My ideal self could not see itself outside of Kansas. I had to realize, through the support of the people I came to know here, that the ideal self that we become is not an identity that we inherit or even follow, it is something we create. The exceptional individual is not a figure outside that we look up to and strive towards, it is the byproduct of a pursuit deep inside us. We are who we are when we live brave lives. When we leave and take a leap. I want to thank everyone here, my advisors, Eckhard Groll, Justin Weibel, Davide Ziviani, and my friends, for being there on the other side of the first, of hopefully many, of my leaps.

"No union is more profound than marriage, for it embodies the highest ideals of love, fidelity, devotion, sacrifice, and family. In forming a marital union, two people become something greater than once they were. As some of the petitioners in these cases demonstrate, marriage embodies a love that may endure even past death. It would misunderstand these men and women to say they disrespect the idea of marriage. Their plea is that they do respect it, respect it so deeply that they seek to find its fulfillment for themselves. Their hope is not to be condemned to live in loneliness, excluded from one of civilization's oldest institutions. They ask for equal dignity in the eyes of the law. The Constitution grants them that right."
Obergerfell v. Hodges

"Ours is a society of written laws. Judges are not free to overlook plain statutory commands on the strength of nothing more than suppositions about intentions or guesswork about expectations. In Title VII, Congress adopted broad language making it illegal for an employer to rely on an employee's sex when deciding to fire that employee. We do not hesitate to recognize today a necessary consequence of that legislative choice: An employer who fires an individual merely for being gay or transgender defies the law."
Bostock v. Clayton County

"And yet when we study the biographies of our heroes, we learn that they spent years in preparation doing tiny, decent things before one historical moment propelled them to center stage. Moments, as if animate, use the prepared to tilt empires."
- Danusha Veronica Goska

TABLE OF CONTENTS

LIST OF TABLES

LIST OF FIGURES

NOMENCLATURE

A	Area (m^2)
a	Acceleration (m/s^2)
c_p	Specific heat at constant pressure (kJ/kg-K)
C	Capacitance (kW/K, F) or coefficient (-)
F	Force (N)
g	Acceleration due to gravity (m/s^2)
I	Current (A)
m	Mass of vehicle (kg)
$\dot{m}$	Mass flow rate (kg/s)
n	Component efficiency (-)
NTU	Number of thermal units (-)
P	Power (W)
Q	Heat generation (W)
R	Resistance (ohm)
UA	Overall conductance (kW/K)
V	Velocity (m/s) or Voltage (V)

Greek symbols

ε	HX effectiveness (-)
η	Surface efficiency (-)
ρ	Density (kg/m^3)

Subscripts

a	Air
$accel$	acceleration
$drag$	drag
$gearbox$	Gearbox
i	Inner (HX)
m	Mixture
max	Maximum
min	Minimum
$motor$	Motor
o	Outer (HX)
OCV	Open circuit voltage
$PWRT$	Powertrain
r	Refrigerant
$roll$	Rolling resistance
$rr,0$	Constant rolling resistance
$rr,1$	Velocity dependent rolling resistance

Acronyms

APM	Auxiliary power modules
BEV	Battery electric vehicle
CSC	Constant speed cycle
ECM	Equivalent circuit model
EXV	Electronic expansion valve
HFEDS	Highway fuel economy drive schedule
HVAC	Heating, ventilation, and air conditioning
HX	Heat exchanger
ICE	Internal combustion engine
MCT	Multi-cycle test
PTC	Positive temperature coefficient
SOC	State of charge
SP	Single polarization
TMS	Thermal management systems
TPIM	Traction power inverter modules
TXV	Thermostatic expansion valve
UDDS	Urban dynamometer drive schedule
VCC	Vapor compression cycle

ABSTRACT

Due to increasing regulation on emissions and shifting consumer preferences, the wide adoption of battery electric vehicles (BEV) hinges on research and development of technologies that can extend system range. This can be accomplished either by increasing the battery size or via more efficient operation of the electrical and thermal systems. This thesis endeavours to accomplish the latter through comparative investigation of BEV integrated thermal management system (ITMS) performance across a range of ambient conditions (-20 °C to 40 °C), cabin setpoints (18 °C to 24 °C), and six different ITMS architectures. A dynamic ITMS modelling framework for a long-range electric vehicle is established with comprehensive sub models for the operation of the drive train, power electronics, battery, vapor compression cycle components, and cabin conditioning. This modelling framework is used to construct a baseline thermal management system, as well as for adaptation to four common systems. Additionally, a novel low-temperature waste heat recovery (LT WHR) system is proposed and shown to have potential benefits at low ambient temperatures through the reduction of the necessary cabin ventilation loading. While this system shows performance improvements, the regular WHR system offers the greatest benefit for long-range BEV drive cycles in terms of system range and transient response. With an optimal thermal management system found for long range BEV's this system is then used as a boundary condition for a study on cooling of the battery. Battery conditioning, health, and as a result their along cell and system lifetime remains an additional concern of consumers as well as thermal systems engineers seeking to ensure safety and ensure longevity of EV battery cells. Three typical coolant flow orientations are studied to compare them under different flow conditions and thermal interface material performance. The battery cooling model is then coupled to the previously established dynamic modelling environment to demonstrate the added modelling capability (and necessity) for incorporating module-level cooling performance in both battery cooling studies and transient ITMS environments.

1. INTRODUCTION

1.1 Battery Electric Vehicles

Battery electric vehicle (BEV) thermal management systems pose unique thermal management challenges compared to traditional internal combustion engine (ICE) vehicles. While the requirements for cabin conditioning are the same, the availability and temperatures of heat sources are radically different. In an ICE, the engine serves as both the source for mechanical power and cabin heating during cold ambient conditions. In a BEV, the engine is replaced with an electric traction motor and large-scale battery system, typically having some variant of Li-ion chemistry [1]. While these BEV systems require active cooling, similar to an ICE, the temperature at which waste heat becomes available is lower, 15-35 °C for battery cooling and 100-120 °C for motor cooling [2], compared to high temperatures of 195 °C present in traditional engines, which also produce more total heat. This lower temperature and availability of waste heat available in BEVs necessitates a supplemental heat source for cabin heating, in addition to the active cooling systems for battery temperature control. This leads to compromised vehicle range, especially under extreme ambient conditions, which is the critical concern of end consumers regarding adoption of BEVs [3].

1.2 Previous Thermal Management and Battery Coolant Flow Studies

Previous analyses of BEV thermal management systems (TMS) typically seek to examine a proposed improvement by building a vehicle and thermal system model to characterize the system response and range benefits. These studies are typically limited to investigation of a single system (or subsystem) with respect to a baseline [4, 5, 6, 7] , a single mode of operation [8, 9], or neglect active battery cooling or heating [4, 8].

Additionally, the extension of this analysis to a battery coolant flow study and optimization is crucial to understand temperature distributions insides cells, a key indicator of long-term cell health, temperature difference within the pack, max battery temperature, and pressure drop inside of the cooling solution. Previous studies on specific battery cooling solutions focus narrowly on a single or small grouping of cells, ignore thermal interface materials (TIM) at key interface points, and ignore fins where applicable in typical module design [13] [14]. These studies are limited to

optimizing a single flow configuration, geometry, or cold plate concept without concern for the broader pack implications.

1.3 Thesis Goals and Scope

The goal of this thesis is to establish a simulation framework to enable comparison across different BEV TMS under common drive cycles, different ambient conditions, and transient control schemes then extend this analysis into a battery coolant flow study and optimization. The results of this flow study are then included into the dynamic thermal system models to show the influence of module performance and system configuration on transient thermal system behavior.

First, a baseline TMS for a long-range battery electric vehicle is established, which provides a standard system for development of the simulation framework in this work, as well as for future performance comparison to alternative TMS architectures. After establishing the BEV TMS, the modeling environment, approach, and assumptions are described in detail, with the goal of establishing the method as a general approach for evaluation of alternate systems. These alternate systems are reviewed and their control is discussed. These models are then used to conduct a parametric study across changing ambient conditions and cabin setpoints in both heating and cooling modes to observe the effects on the overall driving range. Additionally, the transient performance of the implemented control logic in the system is explored for a representative cooling case and heating case.

The completed analysis extends and analyzes six thermal system architectures, across a wide range of ambient temperatures, -20 °C to 40 °C, utilizing a complete ITMS encompassing cabin, power electronics, and battery. The systems are sized and compared for a long-range battery electric vehicle (BEV) across a simulated Multi-Cycle Test (MCT) methodology with the ultimate system range graphed across changing ambient and cabin setpoint conditions while interesting transient results from different flow management scenarios are graphed for consideration. Overall, the most efficient system for long range BEV's is a WHR, positive temperature coefficient (PTC) heater, and HP system when considering long range drive cycles enabled by the systems added range.

The WHR system is then used in a flow study across parameters of flow configuration, volumetric flow rate, inlet temperature, and TIM performance. Finally, these results are imported to the transient modeling environment to demonstrate the coupled nature of module performance

and configuration with transient system control and overall conditioning performance. This coupling is accomplished via a reduced order model of battery module thermal resistance and pressure drop, and an optimal interflow configuration is demonstrated.

2. LITERATURE REVIEW

2.1 BEV Battery Cooling Methods

Electric vehicle batteries and their associated cooling systems have been extensively studied in the literature, as previously exhaustively reviewed in Refs. [1] [10]. The goals of these past studies typically are to optimize existing cooling methods, establish alternate cooling methods, and investigate battery cell architectures.

EV battery cooling methods investigated in the literature include air cooling, liquid cooling, direct refrigerant cooling, and immersion cooling [1] [10]. Air cooling ducts air either from the ambient (passive) or conditioned from the cabin vapor compression cycle (VCC) (active) through the battery. This approach suffers from low cooling capacity due to the poor thermal conductivity of air and the size of the air ducts reduces the effective battery density, both contributing to a decreased range for the finalized system. Thus, air-cooled batteries are typically found in shorter range electric vehicles. Longer range BEVs typically implement liquid cooling due to more favorable heat transfer characteristics that allow for a denser cooling solution. In the case of a direct liquid cooling solution, coolant is brought as close as possible to the battery for optimal heat transfer performance while an indirect solution places a cold plate along the bottom of the entire battery system's length while providing fins to interface with the battery. Further evolutions of direct liquid cooling, seeking improved heat transfer performance to ensure cell safety under extreme conditions, are two-phase direct refrigerant and immersion cooling concepts. Direct refrigerant systems bring two phase refrigerants to the battery via a cold plate and manifold system, like a direct liquid cooling solution, and evaporate the refrigerant. A more uniform and higher capacity cooling are associated with two-phase flow of the refrigerant across the battery cold plate. Passive two-phase immersion cooling submerges the EV battery in dielectric fluid that boils in response to heat rejection from the battery. Currently, these two-phase cooling methods have limited implementation in the consumer market [1] [10]. The current study focuses on ITMS architectures having a secondary loop, indirect liquid cooling system for the battery. Analysis across a wide range of ambient conditions to examine their performance in heating and cooling modes has been identified as a gap in past research [1].

2.2 Battery Cooling

With the modeling methodology and parameters for battery performance reviewed and selected, the literature surrounding coolant flow and optimizations of battery packs is of interest to both define the current modeling space and where it can be extended. In general, flow studies focus on several parameters for optimization, coolant channel geometry, flow orientation, flow rate, and inlet temperature. Typically, module performance is optimized across changing channel geometry or flow orientation, and then the cooling systems' performances are rated across a parametric study of inlet temperature and flowrate conditions. Broadly defined, flow geometries can be defined in two configurations, as shown in Figure 1.

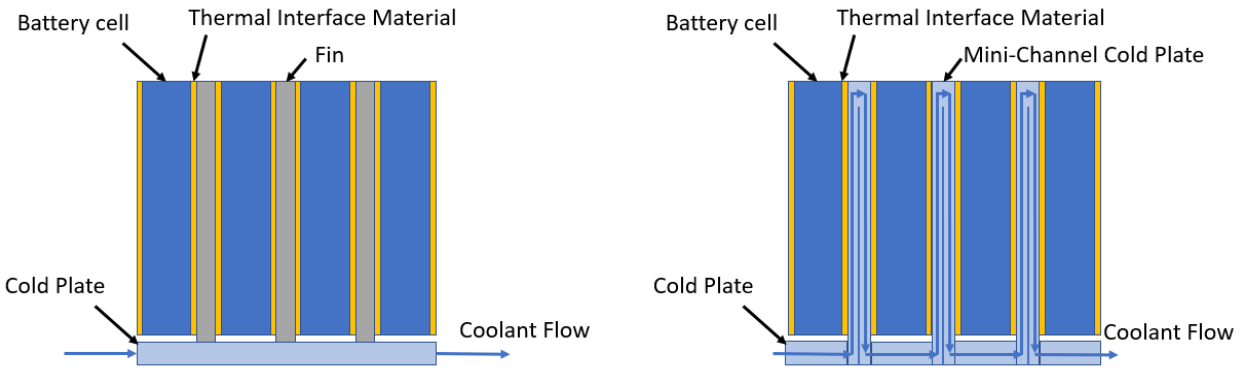

Figure 1: Flow configuration for typical battery coolant flow management study optimizations [1]

In Figure 1a, cooling fins are brought in contact with the battery cell to conduct heat down and to a cold plate with flowing coolant. Typically, in the physical module construction, there is a layer of TIMs between the cells and fins and the fins and cold plate, either a paste or thermal pad [11] [12]. In Figure 1b, the fin concept is eliminated in favor of a mini-channel cold plate cooling concept which brings the coolant directly across the face of the battery cell. This has advantages of reducing the overall use of TIMs and eliminating the use of fins, reducing weight, space, and thermal resistance in the batter pack at the expense of more complicated flow design and increased chances of leaks. This design however does utilize a single layer of TIMs between the cell and mini channel cold plate. In contrast to practical design and construction, many flow studies omit the use of TIMs and fins in their modeling space. [13] [14] [15] [16] [17] [18] [19] This limit to construction is intentional as each of these designs focus more narrowly on a single or small

grouping of cells. A larger grouping of cells necessitates extension of battery pack design to include fins and TIMs at key points, both to accurately characterize the modules performance but also to model it as a useful unit for future transient simulation integration and material study.

2.3 BEV Cabin Conditioning

Heating, ventilation, and air conditioning (HVAC) solutions are critical for all vehicles to ensure consumer comfort across a wide range of ambient conditions. EV cabin cooling solutions mirror those for internal combustion engine (ICE) vehicles [3]. Typical cooling solutions include the use of a traditional vapor compression cycle (VCC), with potential improvements in cooling performance via suction to liquid-line heat exchangers, economization, flash tanks, or vapor injection cooling into modified compressor units. Suction to liquid-line heat exchangers ensures superheat at the compressor inlet while further subcooling the state outside of the condenser; performance enhancements depend upon the type of refrigerant and operating conditions. Economization splits the flow from the condenser and expands it to an intermediate temperature where it is used to further sub cool the remaining flow and provide cooling between stages of compression. This reduces compressor losses while improving the evaporator performance due to the further subcooled liquid state but reduces the mass flow rate to the evaporator and thereby system capacity. A flash tank-based system operates on much the same principles of an economizer, with similar challenges as economization, namely, loss of evaporator capacity, addition of components, overall increase of system charge, and added complexity in control of the system [3].

The design of EV cabin heating systems diverge from ICE vehicles. In ICE vehicles, the large amount of waste heat available from the engine can meet the heating needs of the vehicle even in extremely cold environments. Electric vehicles must rely on alternate forms of heating, such as direct electric heating from positive temperature coefficient (PTC) heaters, heat pumping, fuel-based heaters, or the use of recovered waste heat from the power electronics. Direct electric heating is intrinsically limited to coefficient of performance (COP) of 1, making it a large parasitic draw on the EV traction battery. A heat pump (HP) reverses the flow inside of a typical VCC and rejects heat to the cabin while taking in heat from the ambient. HP heating systems typically suffer from a lack of heating capacity at extremely low ambient temperatures. Fuel heating sources burn an alternate dedicated heating fuel. While this approach overcomes the energy density issue and achieves the necessary heating capacity at extremely low-temperature ambient conditions, it

defeats the original purpose of electrification while increasing the operating costs of the vehicle. [3] Waste heat recovery is the use of waste heat produced by the power electronics for either battery or cabin heating. This heating capacity is essentially free as otherwise it would be dissipated elsewhere in the cabin environment. Various combinations of these heating and cooling systems are investigated as alternate architectures defined later in the paper.

The last remaining components requiring thermal management in an EV are the electric drive systems. These components typically include the auxiliary power module (APM), traction power inverter module (TPIM), and electric motor (EM) [20] [21], which are typically air or liquid cooled [22] [23].

Each of these individual EV subsystems have been extensively investigated in the literature, whereas this current work focuses instead on the modeling of the entire integrated thermal management system (ITMS) for long-range EVs. Within this narrowed scope, ITMS's of varying levels of complexity have been modeled in the literature. Yu et al. [4] established several different EV HP architectures with the goal of finding a more efficient system. The studied architectures were a basic four-component HP system as a baseline, a secondary loop system, and a vapor injection system. Of these, the secondary loop system is proposed in this instance to enable the use of alternate refrigerants, such as R290 and R152a, which pose a risk to passenger safety if allowed to flow inside of the cabin environment. The authors concluded that the R290 secondary loop systems and R744-based traditional heat pump systems provide unique benefits for heating at extremely low ambient temperatures, but that a comprehensive analysis considering both heating and cooling demands was necessary as future work. Wang et al. [24] considered an R134a and R407C air-source HP in heating mode under a range of ambient temperatures from -15 °C to 0 °C. They found that the system can provide adequate heating performance down to an ambient temperature of -10 °C, while experiencing a loss of capacity at -15 °C. This system was not characterized under moderate heating or cooling conditions, and further, did not consider the EV thermal system demands beyond the cabin HVAC needs. Titov and Lustbader [20] comprehensively compared of three thermal management systems: a basic HP system; HP and PTC; and HP, PTC, and waste heat recovery (WHR) in the form of a combined fluid loop (CFL) system. Their analysis, while comprehensive in investigation of the heating cases, did not consider the cooling load or model the battery of the vehicle [20]. Tian et al. [6] analyzed an electric motor WHR system with a HP, the combined benefit of which was analyzed across differing heating and

cooling cases that accounted for the different operating modes of the EV thermal system. The system was simulated across a wide ambient temperature window of -7 °C to 43 °C. Only waste heat from the electric motor, rather than all the power electronics, was considered for recovery.

These reviewed literature analyses range in complexity, from single-cabin models to complete ITMSs. While each of these studies provide insights into segments of specific EV ITMS systems, the current study aims to gain a holistic understanding across multiple systems using a unified modeling framework that accounts for all EV system thermal components, so as to allow for the comprehensive characterization, parametric study, and optimization for different EV design goals. To this end, the current work compares six different thermal system architectures, across a wide range of ambient temperatures from -20 °C to 40 °C, with consideration of the complete ITMS comprising the cabin, electronics, and battery. The systems are sized and compared for a long-range battery electric vehicle (BEV) under a simulated Multi-Cycle Test (MCT) methodology. System performance is quantified based on the ultimate driving range across varying cabin setpoint conditions. The transient system response of the different flow management scenarios is also investigated.

3. METHODOLOGY

This section first introduces the baseline ITMS, main assumptions and governing equations, and boundary conditions. After, the dynamic modeling framework used to predict the performance of the ITMS for a full electric vehicle under a prescribed drive cycle, which was established in a previous study [11], are briefly summarized. Specific updates made to the modelling framework compared to the past work are discussed in further detail; specifically, these updates extend the range of parameterization of the thermal system components and provide validation of the subcomponent models. Implications of the governing assumptions and models are discussed. Next, the modeling methodology surrounding the battery coolant flow study is established. This begins with a review of battery pack construction, coolant flow orientations of interest for study, and the establishment of boundary, parametric, and simulation conditions that define the modeling environment in COMSOL Multiphysics. Finally, a coupling of module-level results is outlined for the modeling of module-level performance in the dynamic Modelica ITMS models [25].

3.1 Baseline Thermal Management System and Modeling Methodology

3.1.1 Baseline Thermal Management System

During earlier stages of this work [26], a baseline TMS was established having the most typical solutions for cabin HVAC, battery thermal management, and electronics cooling for a long-range BEV. The baseline TMS, detailed in Figure 4a, has a standard vapor compression cycle (VCC) that is used for direct cabin cooling and indirect battery cooling via a secondary water-glycol loop. Superheated R134a refrigerant is compressed across a parameterized scroll compressor and then condensed via heat exchange with ambient air. The refrigerant flow splits and can expand across two expansion valves. The first valve (V1) leads to the cabin heat exchanger (HX) while the second valve (V2) leads to the battery HX and cools a secondary water-glycol flow loop that conditions the battery through a cold plate attached to the battery. This secondary pumped loop has an electric heater to heat the battery to an appropriate setpoint in cold conditions, such as an event where the vehicle is cold soaked overnight. The system electronics are cooled through an additional pumped water-glycol loop which reject heat to the air via the radiator [26]. The final system function is the heating of the cabin and battery. Passenger comfort and safety are a function

of heating performance, while the battery short-term capacity and long-term health are improved through proper thermoregulation. Cabin and battery heating are performed via heat sources interfaced with the water-glycol coolant flow for the battery and a secondary liquid-to-air heat exchanger for the cabin environment.

The two system radiators are sized from the overall dimensions of a commercially available radiator based on available engine compartment space, while the cabin and battery evaporator are sized via the ε-NTU method to ensure a minimal footprint within the ducting of the EV's air system. The battery is sized to provide 100 kWh of capacity, which is in line with the goals for a long range EV.

The system control logic follows typical component control schemes using proportional integral controllers. A variable-speed compressor is assumed to be electrically driven rather and controls for the inlet cabin air temperature across the cabin HX. System pumps and fans are controlled to set appropriate battery and cabin mean temperatures, respectively. The two expansions valves for the cabin and battery plate heat exchanger control the evaporator superheat and battery inlet temperature, respectively.

3.1.2 Governing Equations and Assumptions

The modeling approach is detailed here for each of the thermal, mechanical, and control volume systems in the previous section. The transient modeling framework is adopted in the Dymola modeling environment and written in the Modelica language [25]. This environment is multi-disciplinary, covering thermal, mechanical, electrical, and fluid flow systems with defined libraries of components. In this work, the TIL libraries are used to define thermal system components [27]. The modeling environment and specific details on each sub model are described in our previous work [26]. A summary is provided here, followed by further details pertaining to extension and verification of the model later in Section 2.2.

Beginning first with the drive train model, a force balance on an electric vehicle subject to the force required for scheduled vehicle acceleration (F_{accel}), drag (F_{drag}), and rolling friction (F_{roll}) is considered. The total force required from the powertrain (F_{PWRT}) is thereby calculated using the following equations:

$$F_{roll} = \left(C_{rr,0} + C_{rr,1}V\right)mg \tag{1}$$

$$F_{accel} = ma \tag{2}$$

$$F_{drag} = \frac{1}{2}\rho A C_{drag} V^2 \tag{3}$$

$$F_{PWRT} = F_{roll} + F_{accel} + F_{drag} \tag{4}$$

where $C_{rr,0}$ is a constant rolling resistance, $C_{rr,1}$ is the velocity dependent rolling resistance, ρ is the density of air, C_{drag} is the drag coefficient, and A is the front facing area. Assumed parameters for vehicle mass, drag, and rolling resistance are summarized in Table 1. The density of air is calculated according to the ambient conditions.

Table 1: Assumed parameters for vehicle drivetrain modeling

Parameter	**Value**	**Unit**
m	2000	kg
g	9.81	m/s^2
$C_{rr,0}$	0.01	-
$C_{rr,1}$	0.000225	-
A	2.23	m^2
C_{drag}	.27	-

This model then sets the total vehicle power requirements as a function of the input drive schedule which in turn sets the power draw for the power electronics model.

The power electronics model is a black box model using singular constant efficiencies [26] to approximate both the power requirements experienced by each component and the total heat generation during a drive cycle. The power electronics include the electric machine or motor (EM), traction power inverter module (TPIM), and the auxiliary power module (APM). Each electronics component is parameterized as a heat source, adding heat to the liquid cooling loop defined in the baseline architecture via the TIL libraries [27]. These heat losses are assumed as component-level efficiencies which multiply together to increase the power demand on the system and produce heat generation in electrical components as

$$F_{PWRT} \cdot V = P_{TPIM} n_{TPIM} n_{motor} n_{gearbox} \tag{5}$$

$$Q_x = P_x \cdot (1 - n_x) \tag{6}$$

where the subscript x indicates either the motor, gearbox, or TPIM. The assumed system efficiencies for the power electronics components, motor, and gearbox are identified in Table 2, along with the original source.

Table 2: Assumed power electronics efficiencies

Parameter	Value	Source
n_{TPIM}	0.963	[28]
n_{motor}	0.95	[29]
$n_{gearbox}$	0.98	[30]
n_{APM}	0.9	[31]

The battery pack is parameterized as a grouping of individual prismatic cells in line connected via defined series and parallel connections. The electrical side of the battery model is parameterized as an equivalent circuit model (ECM). The battery ECM considered is a single polarization (SP) model (i.e., Thevenin equivalent circuit). This SP model has an open circuit voltage paired with an internal resistance, R_0, and a RC pair, R_1 and C_1 [29], as shown in Figure 2.

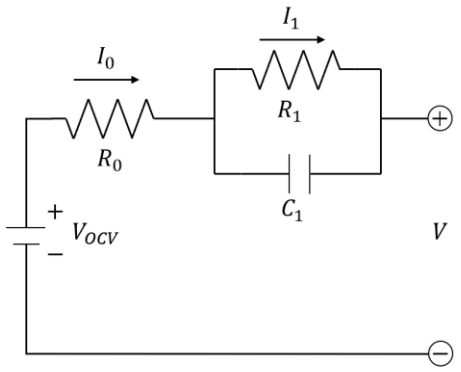

Figure 2: Circuit diagram of a single polarization (SP) equivalent circuit model (ECM) for the battery.

To approximate the batter pack behavior, each module scales with electric circuit parameters according to the user-defined discretization. Moreover, on the thermal side, the batteries are considered as two-dimensional thermal models with user-defined parameters for conductivity and thermal capacity to match.

Open literature was surveyed to select the parameterized ECM for the battery. The findings of the literature review are summarized in Table 3. The studies reviewed were categorized based on several of important characteristics which indicate if the data can be utilized for the purposes of developing a battery ECM for transient thermal management investigations. These characteristics (the columns in Table 3 include the: cell geometry; equivalent circuit type (single polarization (SP) or dual polarization (DP)); whether the reported parameters are temperature-dependent, state of charge (SOC)-dependent, or state of health (SOH)-dependent; whether cell thermal properties such as thermal capacity, weight, or conductivity are provided; the parameterized temperature range; specified test conditions for replication and verification of the results of the paper; and finally, whether the necessary circuit parameters are reported. A priority criterion for this survey was the desire to have a temperature range that extended down to -20 °C, an important extreme condition for evaluation of the ITMS architectures explored in this work. Of the models that cover such a temperature range [32] [33] [34], key parameters such as necessary cell geometry [32], upper temperature range [33], and cell thermal parameters [34] are missing to develop a complete ECM. For this reason, a cell parameterization with the complete information [35] but a narrower temperature range (40 °C to 5 °C) is adopted and used down to -20 °C by holding the resistance constant at low temperatures (5 °C to -20 °C) . Conclusions for the open parameterization of battery data to enable more and more in-depth studies of EV TMS. With this the battery heat generation is established which then interfaces through the secondary loop architecture with the VCC.

Table 3: Review of parameterized battery equivalent circuit models

Cell Geometry	Model	Temperature Dependent	SOC	SOH	Cell Thermal Properties	Temperature Range	Test Conditions	Circuit Parameters	Source
Cylindrical	DP	No	Yes	NA	No	NA	Yes	Yes	[36]
NA	DP	No	Yes	NA	No	NA	Yes	Yes	[37]
NA	DP	Yes	Yes	NA	No	(45 °C to -5 °C)	Yes	NA	[38]
NA	SP	Yes	Yes	NA	No	(50 °C to 5 °C)	Yes	NA	[39]
Cylindrical	DP	Yes	No	NA	Yes	(40 °C to 10 °C)	Yes	Yes	[40]
Cylindrical	SP	Yes	Yes	NA	No	(40 °C to 0 °C)	Yes	Yes	[41]
Cylindrical	DP	Yes	Yes	NA	No	(45 °C to 15 °C)	Yes	Yes	[32]
NA	DP	No	Yes	NA	No	yes	Yes	No	[42]
Prismatic	DP	Yes	Yes	NA	No	(45 °C to -5 °C)	Yes	No	[43]
Prismatic	DP	Yes	Yes	NA	No	(55 °C to 0 °C)	No	Yes	[44]
NA	DP	Yes (NA)	Yes	NA	No	no	Yes	No	[45]
NA	DP	Yes	Yes	Yes	No	(45 °C to 5 °C)	Yes	Yes	[46]
Prismatic	SP	yes	Yes	NA	Yes	(20 °C to -20 °C)	Yes	Yes	[33]
Pouch	NA	Yes	Yes	NA	No	(25 °C to -20 °C)	Yes	No	[34]
Prismatic	SP	Yes	Yes	NA	Yes	(40 °C to 5 °C)	Yes	Yes	[35]

Heat transfer calculations are executed dynamically throughout the cycle run time by a set of heat transfer correlations implemented in heat exchanger models utilizing finite volume formulations. The fluids type, components, and selected correlations are summarized in Table 3. Overall, outside finned surface area efficiencies of 90% are assumed with no pressure drop inside of heat exchangers refrigerant lines.

There are several heat exchangers that must be sized to ensure performance of the system. These include the cabin evaporator, cabin heat exchanger (HX), battery plate HX, and two ambient radiators. The inside area, outside area, and overall dimensions for each heat exchanger are summarized in Tables A3 to A6 in the Appendix.

For the cabin evaporator and cabin HX, the ε-NTU method is used to find the minimum area needed to meet the specified sizing condition while meeting a target effectiveness ε. For the cabin evaporator a set amount of superheat, 8 K, at the outlet is ensure during cooling mode. The setpoint of the PTC liquid temperature and flowrates of coolant and air dictate the cabin HX size during heating mode.

The model divides the HX into segments depending on whether there are single-phase or two-phase flow conditions locally. For single-phase regions, the governing equations below are applied for a predefined effectiveness relation in cross flow. The air is considered to be mixed while the refrigerant is unmixed.

$$NTU = \frac{UA}{C_{min}} \tag{7}$$

$$C_{min} = \min(\dot{m}_a c_{pa}, \dot{m}_r c_{pr}) \tag{8}$$

$$C_{max} = \max(\dot{m}_a c_{pa}, \dot{m}_r c_{pr}) \tag{9}$$

$$C^* = \frac{C_{min}}{C_{max}} \tag{10}$$

$$UA = \left((\eta_o h_o A_o)^{-1} + (h_i A_i)^{-1}\right)^{-1} \tag{11}$$

When C_{max} is mixed:

$$\varepsilon = 1/C^* \cdot \left(1 - exp\left(-C^* \cdot \left(1 - exp(-NTU)\right)\right)\right) \tag{12}$$

When C_{max} is unmixed:

$$\varepsilon = 1 - exp\left(-\frac{1}{C^*} \cdot \left(1 - exp(-C^* \cdot NTU)\right)\right) \quad (13)$$

In two-phase regions, the governing equations are:

$$\varepsilon = 1 - e^{-NTU} \quad (14)$$

$$NTU = \frac{UA}{\dot{m}_a} \quad (15)$$

$$UA = \left(\frac{c_{p,m}}{\eta_o h_o A_o} + \frac{c_c}{h_i A_i}\right)^{-1} \quad (16)$$

A target effectiveness is set as 0.75 which determines the number of thermal units, NTU, for the heat exchanger. This is then used to determine the overall conductance, UA, of the heat exchanger in dependence of the inside area, A_i, and outside areas, A_o. Following this approach, the area for a heat exchanger can be minimized through optimization of these governing equations. Sizing of the components is performed via steady state simulation at 48 kph (30 mph), at 35 °C for the cabin evaporator and at -10 °C for the cabin HX.

The ambient radiator sizing is a tradeoff between available space inside of the engine compartment and cooling capacity of the system. Because the size of an engine compartment is not considered, the radiator size for the VCC cycle and power electronics cooling loop is based on a typical size of a commercial ambient radiator.

The battery plate HX is separately sized based on the heat load predicted by the battery ECM. The heat exchanger is sized to ensure a minimum amount of battery evaporator superheat, 8 K, at 48 kph (30 mph) and 35 °C cooling case.

Table 4. Heat transfer fluids, components, and correlations used for single and two-phase flow

Heat Exchanger	Fluid	Single Phase Correlation	Two-Phase Correlation
Cabin Evaporator	R134a	[47, 48]	[50, 51]
	Air	[49]	N/A
Battery Evaporator	R134a	[47, 48]	[52]
	Water Glycol	[47, 48]	N/A
Cabin HX	Air	[53]	N/A
	Water Glycol	[47, 48]	N/A
VCC Radiator	Air	[47, 48]	N/A
	Water Glycol	[49]	N/A
VCC Radiator	R134a	[47, 48]	[54]
	Air	[49]	NA

The compressor parameterization adopted in modeling the baseline system in our previous work assumed fixed isentropic, volumetric, and overall isentropic efficiencies [26]. This assumption, while common for preliminary component sizing, fails to capture key trends in compressor performance, namely, the decreased heating capacity of heat pumps at extremely low ambient temperatures on the order of -10 °C to -20 °C. To capture this key compressor trend over a wide range of ambient conditions AHRI mapping coefficients [55] were used to directly parameterize a compressor from a manufacturer.

$$\left(\dot{W}_{map}, \dot{m}_{map}\right) = C_1 + C_2 \cdot T_{\text{evap}} + C_3 \cdot T_{\text{cond}} + C_4 \cdot T_{\text{evap}}^2 + C_5 \cdot T_{\text{evap}} \cdot T_{\text{cond}} + C_6 \cdot T_{\text{cond}}^2 + C_7 \cdot T_{\text{evap}}^3 + C_8 \cdot T_{\text{evap}}^2 \cdot T_{\text{cond}} + C_9 \cdot T_{\text{cond}}^2 \cdot T_{\text{evap}} + C_{10} \cdot T_{\text{cond}}^3 \quad (10)$$

This approach has distinct advantages over alternative approaches. Firstly, the compressor can be sized to specific conditions for the cabin and battery system. Second, the compressor, and resulting compressor envelope, can be selected such that it covers the necessary operating conditions across a wide range of ambient temperatures. The compressor modeled in this study (Emerson ZS38K4E-PFV) is selected to provide a target capacity of 6 kW of cooling at an ambient temperature of 35° C. This compressor speed is controlled with a proportional integral (PI)-controller based on an assumed maximum input taken from the compressor specifications.

$$\dot{m}_{comp} = \dot{m}_{map} \frac{N}{60} \quad (11)$$

$$\dot{W}_{comp} = \dot{W}_{map} \frac{N}{60} \quad (12)$$

The mapping adopted from the compressor manufacturer was constructed under a fixed superheat of 11.11 K which will not necessarily always be the case when simulating the system under transient operating conditions. These deviations are considered in the final governing equations for the compressor model by setting the factor f to 0.75 in the following corrections:

$$\dot{m}_{new} = \dot{m}_{comp}\left(1 + f \cdot \left(\frac{\rho_{suc,new}}{\rho_{suc,data}} - 1\right)\right) \quad (13)$$

$$\dot{W}_{new} = \dot{W}_{comp}\left(\frac{\dot{m}_{new}}{\dot{m}_{comp}} \cdot \frac{\Delta h_{s,new}}{\Delta h_{s,map}}\right) \quad (14)$$

It is further assumed that the compressor work is transferred to the refrigerant to fix the outlet state.

From the VCC, heat is extracted from the air recirculating from the cabin, mixing with fresh ventilated air from the ambient environment. The cabin model is coupled with an ambient weather model that has user-defined inputs that allow consideration of variations in ambient temperature, air density, humidity, precipitation, wind, and sun position and intensity. For the purposes of this study, only the ambient temperature is varied as indicated alongside the results of each parametric condition. A sunny day is assumed at each ambient temperature with no wind and a humidity of 50%. A direct solar flux is set to 600 W/m^2 with a diffuse solar flux of 200 W/m^2. The recirculation is controlled to 80% fresh air and 20% recirculated air for each simulated condition heating condition while the recirculation ratio is varied to meet cooling performance; up to 40% recirculated air as fogging is not a concern.

It is important to verify that the cabin parameters considered in the model predict the imposed heat load within realistic expectations for a consumer long-range EV. To verify the cabin model, predictions are compared to other literature solutions [4] [57] across three control variables: outdoor temperature, recirculation ratio, and solar flux. It is important to note that the cabin model parameters from the TIL libraries are kept as default and no specific cabin parameters from past literature sources have been adopted. This is done because past literature solutions offered incomplete data that would be required for a full parameterization, often neglecting to provide the cabin air volume, key dimensions, or materials and material properties. The comparison across the stated control variables therefore aims to verify the magnitude and trend of the imposed cabin heat loading, rather than achieve an exact match with literature.

The verification of these loadings is completed for specific cases available from the original literature data, which typically characterize the total cabin heating load or decomposes the total into the ventilation and ambient loading. The input parameters for these simulations are shown in Table 5, which consider variations in the ambient temperature, recirculation ratio, and solar flux.

With variation of the ambient temperature, the bar chart in Figure 3a shows that the predicted steady state ventilation and ambient loadings match well with the literature, capturing the trend of decreasing heat loads with increasing ambient temperature and matching the magnitudes. For the variation in recirculation ratio, shown in Figure 3b, the current simulations and literature data also agree, capturing both the magnitude and trend of the total heat load. Finally, the variation with solar flux is shown in Figure 3c, capturing both trends and magnitudes.

Table 5: Cabin validation simulation cases for variation in the ambient temperature, recirculation ratio, and solar flux.

Cabin (°C)	Ambient (°C)	Solar Flux (W/m^2)	R (%)	V_{flow} (m^3/s)
Ambient Temperature Variation				
24	0	NA	0%	0.07
24	-10	NA	0%	0.07
24	-20	NA	0%	0.07
Recirculation Ratio Variation				
24	-10	NA	0%	0.07
24	-10	NA	20%	0.07
24	-10	NA	30%	0.07
Solar Flux Variation				
22	43	0	30%	0.045
22	43	1000	30%	0.045

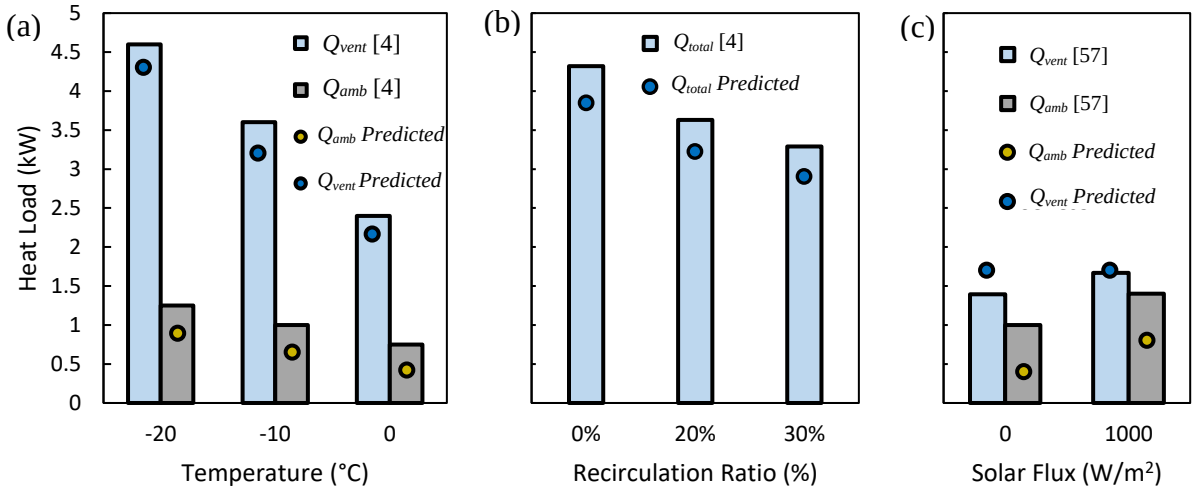

Figure 3: Comparison of the predicted cabin heat loads (dots) versus literature data (bars) for a variation in (a) ambient temperature, (b) recirculation ratio, and (c) solar flux. The heat load is either shown as the total (Q_{total}), ventilation load (Q_{vent}), or ambient load (Q_{amb}).

3.2 BEV TMSs Considered

In addition to the baseline described above five additional thermal management system architectures to be analyzed are described in the following subsections. Each of these architectures

share similar thermal systems components with the baseline, with modifications that increase the complexity of the VCC or water-glycol flow control systems. Each system description that follows begins at the inlet to the compressor and continues around the various thermal management loops, highlighting key control logic and differences in the architecture.

3.2.1 Baseline with Low Temperature (LT) Radiator: "LT-HX"

The first additional system considered is the baseline system with the addition of a low-temperature radiator for battery cooling and an internal heat exchanger to the VCC, shown in Figure 4b. The proposed advantage of this system is the extension of system range through low-temperature cooling of the battery. At low ambient temperatures when the cabin environment would not need to be cooled, while the battery may still need cooling after a long drive cycle to be to maintain it in its thermal limits. This system would allow for the VCC to be decoupled from battery cooling, thus saving overall energy. Additionally, the added internal heat exchanger would further subcool the condensed refrigerant exiting the radiator while ensuring compressor safety.

Starting at the inlet to the compressor, superheated vapor is compressed to a high temperature and then condensed across an ambient radiator until it exits in a subcooled condition. Here it enters the tube-in-tube internal heat exchanger where it is further subcooled by cold vapor leaving the evaporators. After expanding across a thermostatic expansion valve (TXV), the refrigerant diverts to either the cabin or battery evaporator. Exiting each evaporator, the two streams of vapor mix until they are further superheated as they pass through the cold side of the tube-in-tube heat exchanger to ensure compressor safety. In the secondary liquid cooling loop for the battery, beginning at the inlet to the battery cold plate, a water glycol mixture cools or heats the battery and enters a valve controlled (V3) split in the flow. When the battery is hotter than the ambient, flow is directed to a front-end radiator for low-temperature heat rejection. When the battery is above its setpoint temperature or when it is below the ambient condition, the valve directs the coolant through the battery evaporator. The water glycol loops for the power electronics cooling and cabin heating remains unchanged from the baseline.

3.2.2 Heat Pump (HP): "HP"

A heat pump system (Figure 4c) is also considered to eliminate the need for the cabin PTC heater, as the heat pump operates at an inherently higher COP than the electric heater. From the inlet to the compressor, superheated vapor is compressed to a high-pressure state where it encounters a four-way valve (V4) that is actuated based on the mode of the VCC system. For cabin cooling, the valve position is such that the VCC system operates identically to the baseline, where the front-end heat exchanger acts as a condenser and the cabin heat exchanger acts as an evaporator. For cabin heating, the refrigerant flow is reversed by the four-way valve. In this mode, the high pressure and temperature vapor exiting the compressor flows through the cabin heat exchanger, which now acts a condenser. During this heating mode of operation, the battery flow control valve (V2) is closed to prevent flow through this loop. Once the refrigerant condenses, it flows through the expansion valve (V1) and into the front-end radiator where it evaporates. The system diagram for the battery and power electronics cooling loops remains unchanged from the baseline system. The four-way valve is controlled such that it switches at a balance point of 21 °C ambient between heating and cooling modes. The balance point here is the point where conditioning demand switches from heating to cooling and vice versa based on ambient temperature.

3.2.3 Heat Pump and Positive Temperature Coefficient (PTC) Heater: "HP&PTC"

The next system considered is the heat pump system without elimination of the cabin PTC heater, shown in Figure 4d. The PTC heater can thereby compensate for capacity losses experienced by the heat pump at low ambient temperatures. The vapor compression systems remain unchanged from the heat pump diagram, but the cabin water-glycol heating loop from the baseline is added in tandem to the cabin heat exchanger to provide additional capacity during high-demand scenarios. The system control is modified from the baseline and heat pump systems because the VCC compressor and the PTC heater would both typically control for the same inlet temperature to cabin environment. The HP, with an inherent COP greater than 1, is preferred to the electric heater for the cabin. To ensure that the electric heater is shutoff as soon as possible in the transient cycle a limit is placed on the control of the compressor unit for the heat pumping mode. During heating action, if any electric heating power above a threshold of 50 watts is being used, the compressor would be operated at maximum capacity or full speed by default. This would

allow for the electric heater to fluctuate during transient heat up periods to control the cabin inlet temperature. Once the high demand heating up period is finished, the electric heater would fall below the threshold value and the compressor would be controlled to set the cabin inlet temperature during steady operation. This control logic is maintained and expanded upon in the next two architectures and its implementation is referenced from Titov and Lustbader [20].

3.2.4 Heat Pump, PTC, and Waste Heat Recovery (WHR): "WHR"

The next system is a modification of the previous HP and PTC system presented in Section 3.3, with additional flow control that allows for the recovery of waste heat from the power electronics for the purposes of heating the battery or the cabin. The primary components that make up this system remain unchanged from the HP and PTC system, with only the addition of flow control valves that connect the power electronics water-glycol cooling loop to the cabin and battery water-glycol loop. Beginning at the inlet to the TPIM in Figure 4e, the water glycol cools each of the electronic components and exits to a four-way valve (V5). This valve can either place the power electronics loop in series with the secondary loop for battery heating or maintain these as independent pumped loops. After either flowing through or bypassing the battery loop, the flow then passes to a second additional four-way valve (V6). This valve can similarly either place the power electronics in series with the cabin heating loop or bypass this cabin loop. Together, these valves allow waste heat from the power electronics to supplement necessary heating for the battery (V5) or cabin (V6). Finally, after either bypassing or flowing through the cabin heat exchanger, the water glycol flow comes to a simple bypass valve (V7) which plays a critical role in maintaining the temperatures of both the power electronics and the cabin environment. The valve operates to bypass the front-end radiator where the power electronics waste heat would typically be dumped to the environment if not being recovered.

Adding another potential heat source to control for the cabin inlet temperature in the architecture, in addition to the HP and cabin PTC, leads to three potential heat sources for controlling this variable at a given time. A layered control scheme is adopted from the CFL system investigated in the literature [20]. The control scheme considers the most efficient heat source as the waste heat recovered from the power electronics, followed by the heat pump, and finally the PTC heater. The control scheme works to use PTC power only when necessary during high demand periods. Once it falls below a threshold value of 50 W, compressor speed is controlled to ensure

cabin conditioning. Finally, once the compressor speed falls below a threshold value of 5 Hz, the bypass valve then works to ensure the cabin inlet temperature by proportionally bypassing flow from the exchanger in a range of 0% to 100%. Additionally, the bypass valve operates to ensure the temperature of the power electronics. If at any point during heating operation the power electronics go above a safety threshold of 120 °C, the bypass engages to cool the power electronics over a 5 min period. This bypass mode, while available, is not typically engaged as the partial bypass flow for cabin heating regulates that either waste heat is being directed to the cabin or the environment in periods of low heating demand. Regardless, with potentially three separate controllers available for a single bypass valve appropriate time constants and smoothing functions must be applied to eliminate local maxima and minima present during simulation. A time-averaged mean is applied to each mode-control variable as they are passed to the PI controllers for each component. These mode-control variables are the PTC power, compressor speed, and power electronics temperature. Additionally, whereas modeling in the baseline system assumed the power electronics to be black-box efficiency models, parameterized thermal masses are added to the updated systems to ensure temperature fluctuations from the thermal system do not inadvertently trigger flow control logic. Finally, the remaining control logic governs actuation of the four-way valves that place the water glycol loops into series or bypass modes. For the battery flow control valve (V5), the control variable is the mean temperature of the battery; once heated to a lower temperature threshold of 15 °C, the four-way valve actuates to bypass the battery. This removes the heating load of the battery and increases the available waste heating capacity for the cabin. The cabin four-way flow control valve (V6) is actuated based upon the balance point temperature for system heating or cooling. In this way, whenever the ambient temperature is below the threshold of 20 °C waste heat is recovered to offset necessary electrical input.

3.2.5 Heat Pump, PTC, WHR, and Low-Temperature (LT) WHR: "LT-WHR"

The following novel system architecture operates much the same way as the previous system (Section 3.4), utilizing a combination of HP, PTC, WHR, but with the addition of low-temperature (LT) WHR. This architecture seeks to utilize the EV battery as another potential source of waste heat. Typical Li-ion batteries operate in a rather narrow band of temperatures from 15 °C to 35 °C, which does not offer a substantial temperature difference for meaningful recovery considering cabin setpoints from 18 °C to 24 °C. There is however a potentially larger temperature difference

available for heat exchange with incoming fresh air that is necessary to prevent fogging, especially during extremely low ambient conditions, which could offer a meaningful opportunity for LT WHR. This is achieved in the system (Figure 4f), via an additional air to water-glycol heat exchanger in the battery secondary loop, which would be ducted with fresh air to extract waste heat from the battery once within its safe operating temperature range. Additionally, a final bypass valve (V8) is added to route coolant through the appropriate heat exchanger based upon mode selection. These modes are determined by the operating temperature limits of the battery; the four-way valve (V4) is switched first to take the battery secondary loop out of series with the power electronics. Then, after a 100s wait period, the battery coolant is directed through the LT HX and conditions the incoming fresh air into the system.

3.2.6 Summary of Control Variables and Targets

All the control logic for each system is summarized in Table 6. Across heating and cooling cycles the systems actively control for battery mean temperature, battery inlet temperature, cabin mean temperature, and cabin inlet temperature.

Table 6: Independent and dependent control variables for thermal system components

Component	Architecture	Control Variable	Value	Dependent Variable
V1	All	Cabin Evaporator Superheat	5 °C	Evaporator Cooling Capacity
V2	All	Battery Inlet Temperature	User Chosen	Battery HX Capacity
V3	LT-HX	Battery Mean Temperature	User Chosen	Battery Flow Direction
V4	HP, HP&PTC, WHR, LT-WHR	Ambient Temperature	21 °C	VCC Flow Direction
V5	WHR, LT-WHR	Battery Mean Temperature	15 °C	Battery WHR Flow Control
V6	WHR, LT-WHR	Ambient Temperature	21 °C	Cabin WHR Flow Control
V7	WHR, LT-WHR	Electronics Temperature	120 °C	Electronics Flow Control
V8	LT-WHR	Battery Mean Temperature	15 °C	Battery LT-WHR Flow Control
C1	All	Cabin Inlet Temperature	User Chosen	VCC System Capacity
P1	All	None		Electronics Mass flow
P2	All	None		Cabin heater Mass flow
P3	All	Battery Mean Temperature	User Chosen	Battery Coolant Mass flow
F1	All	None		VCC Radiator Volume flow
F2	All	Cabin mean Temperature	User Chosen	Cabin air Volume flow

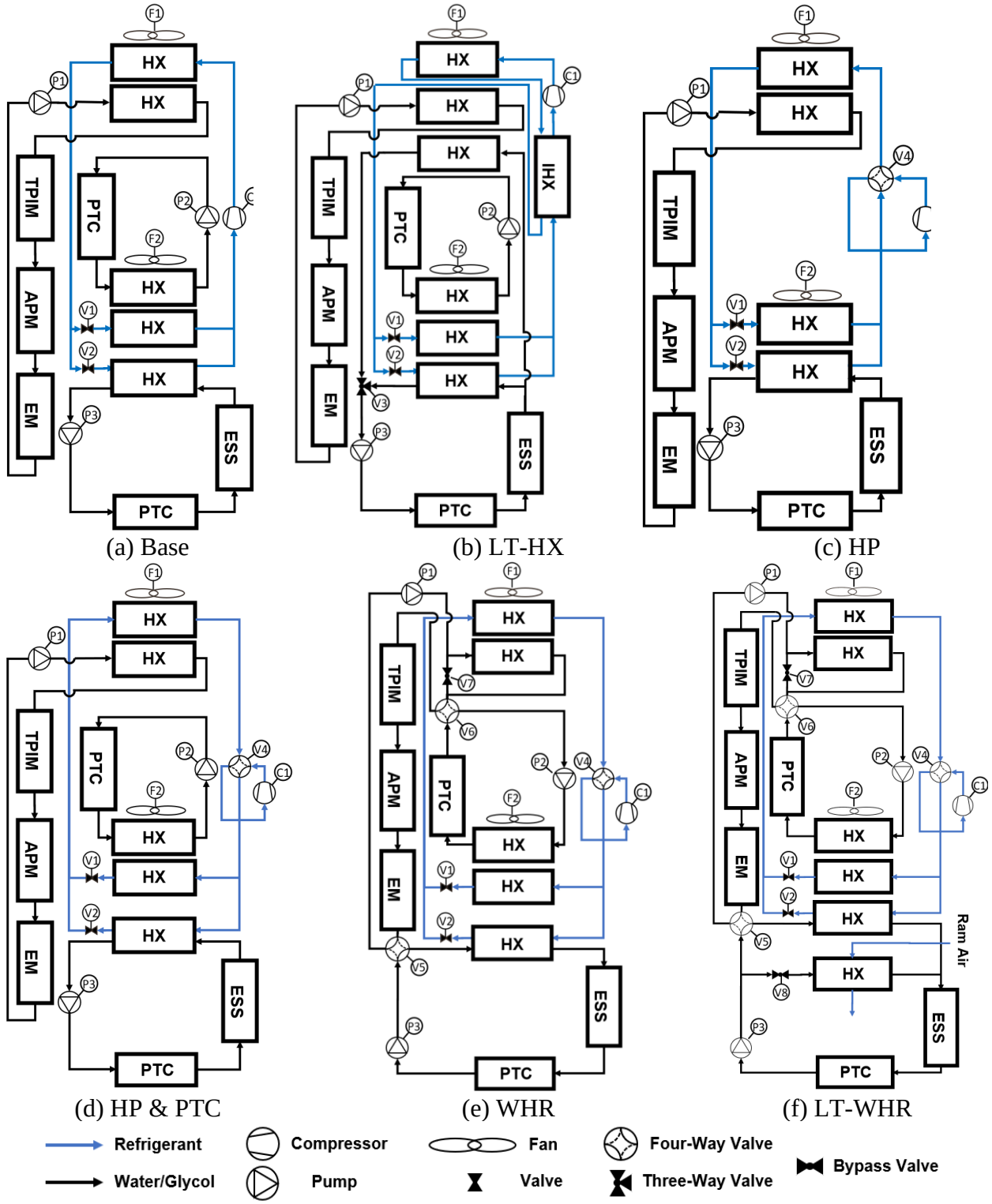

Figure 4: Schematic flow diagrams of all battery electric vehicle (BEV) integrated thermal management system (ITMS) architectures: (a) Baseline (Base), (b) Baseline with low-temperature radiator (LT-HX), (c) Heat pump (HP), (d) Heat pump and PTC heater (HP&PTC), (e) Heat pump, PTC, and waste heat recovery (WHR), and (f) Heat pump, PTC, WHR, and low-temperature WHR (LT-WHR).

3.3 ITMS Simulation Methodology

This section outlines the critical boundary and initialization conditions, including boundary conditions for the ambient and vehicle velocity. The transient initialization strategy is discussed in the context of system charge, pressure initialization, PI control initialization, and the initialization of the system as it transitions between heating and cooling mode. Finally, the simulation test cases to be examined across the different ITMS architectures are outlined.

3.3.1 ITMS Boundary Conditions

Ambient conditions can be provided either at various times of a parameterized day (including the precipitation, wind speed and direction, and changing sun condition and position) or under fixed conditions held constant throughout the simulation. For the purposes of this study, fixed conditions are assumed with the vehicle driving north with no wind on a clear sunny day, at constant ambient temperature, humidity, and the resulting air psychrometric properties. The vehicles cabin is exposed to direct and diffuse solar radiation of 600 and 200 W/m^2, respectively. The constant ambient temperature is varied parametrically between each case across a range of -20 °C to 40 °C.

The vehicles velocity schedule is defined by the time varying input of a multi-cycle test (MCT) [58] methodology, as described in detail in the preceding work [26]. In practice, this cycle is designed to avoid long dynamometer schedules experienced when testing the ranges of long range EV's. Under previous testing schemes classic rating cycles such as HWFET and UDDS drive schedules would need to be repeated tens of times to fully deplete the EV battery and reach end of test condition. The MCT methodology is designed to examine high and low charge dynamics while shortening overall testing time via high constant speed cycles which drain the battery quickly. This provides benefit for simulation time as well leading to shortened simulation time overall.

3.3.2 ITMS Initialization Conditions

As the model is transient in nature, initialization conditions must be specified to pose the problem to be solved by the numerically. The initial conditions include pressure and temperature initialization for the VCC equipment and fluid, temperature initialization conditions for solid

thermal masses in the system, and initial temperature for the cabin volume. For the VCC, low- and high-side pressures of the compressor are initialized at 500 kPa and 1200 kPa, respectively, for all simulations across heating and cooling modes. To ensure a consistent system charge independent of the enthalpy or temperatures inside the VCC loop, a controller for system charge is introduced. This controller acts as a point source or sink where refrigerant mass can enter or exit the system. For the purposes of this simulation the system charge is set to 0.75 kg. The thermal masses throughout the system include the battery, power electronics, cabin component, heat exchangers, and the various fluids (water/glycol, mixed air, refrigerant). A soak initialization condition is chosen such that the thermal masses inside of the system are initialized at the ambient temperature for the test condition. The battery is initially charged to SOC = 0.95 with an initial current of zero. For the water glycol circulating loops the PI controls are initialized at 0.25 kg/s while the compressor and mass flow through the VCC system are initially shutoff.

3.3.3 ITMS Parametric Simulations

The simulated conditions sweep across a range of ambient temperatures, cabin set point temperatures. Battery setpoint temperatures following logical temperatures in heat and cooling modes were also initially investigated, but they caused no appreciable difference on system range. Test cases are performed at fixed ambient temperatures of -20 °C , -10 °C , 0 °C , 10 °C , 25 °C , 30 °C , and 40 °C . At each ambient temperature, the cabin setpoint is evaluated at 18 °C , 20 °C , 22 °C , and 24 °C . The cabin setpoints determine the heating or cooling targets of the system across the simulated MCT cycle. All of the ITMS architectures are evaluated across all setpoint combinations; cases where specific system architectures fail to achieve these targets are discussed in the results. The achievable driving range and transient performance is compared across each system architecture for cases where the setpoints can be achieved. During heating simulation cases the battery setpoint is 15 °C and during cooling cases the battery is set to 35 °C.

3.4 BEV Battery Coolant Flow Modeling and Simulation Methodology

After the determination of an optimal thermal management system several boundary conditions are taken from the transient thermal model to be used as boundary conditions for the

battery coolant flow study. These are the maximum flow rate, inlet temperature range, rating current, and battery pack configuration.

3.4.1 Pack Construction and TIM location

Beginning with a review of pack construction, a bundle of cells (called a unit of cells) is considered. This is shown in Figure 5. This unit consists of 8 cells with parallel electrical connections or 8p connections. This 8p unit is then assembled into a module with 5 of these 8p units in series or 5s. The final module configuration is then termed 5s 8p as shorthand and is shown in Figure 5. Examining the construction, a representative section shows the cold plate interfaced, via TIM, with a set of fins, which then interface to the batteries via another layer of TIM. This pattern repeats throughout the module allowing for the interconnected thermal mass of the batteries to act to redistribute heat load throughout while heat is conducted from the battery through a TIM layer, known hence as *Fin TIM* through the fin down to the cold plate through a final layer of TIM, the gap pad TIM referred to hence as *Gap TIM*. Heat is then conducted into the cold plate and cooled convectively by a flowing stream of coolant.

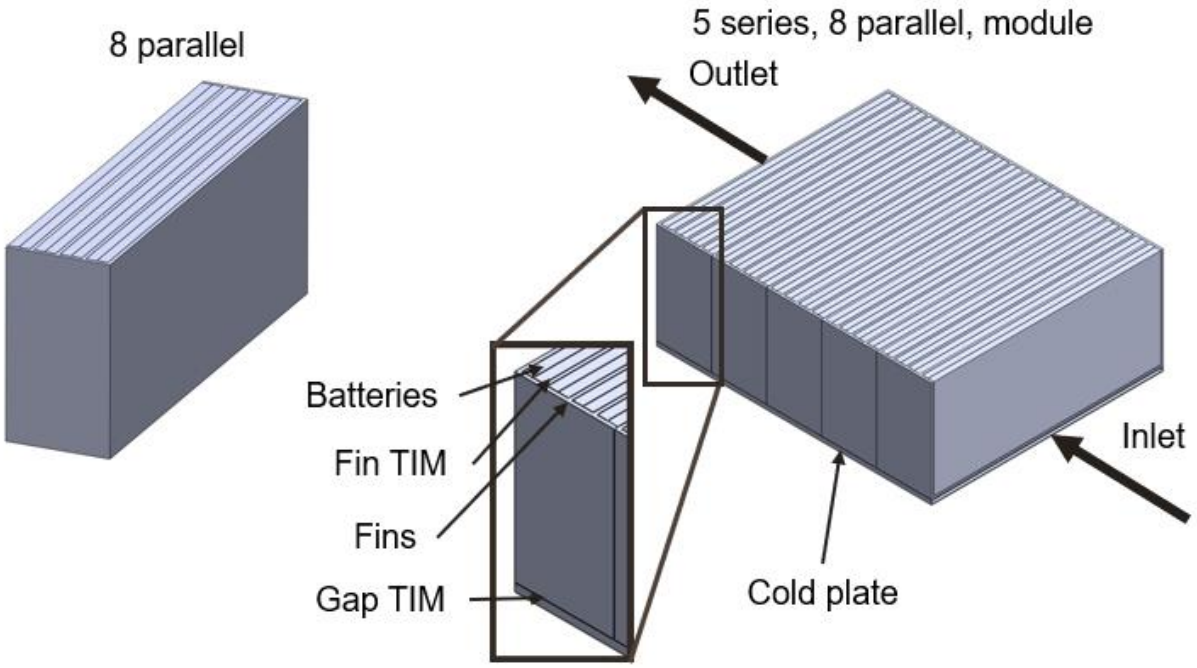

Figure 5: 5s 8p module configuration and construction diagram

3.4.2 Module Flow Configuration

With the pack fully constructed, the flow configurations are outlined. The first, shown in Figure 6a, is the Straight Channel (SC) flow concept that places a single channel with flowing coolant passing across the bottom of the battery cells. This is a typical flow configuration due to its simple construction and flow domain. This concept will be studied here as a baseline case to rate module performance and compare to future enhancements to the module structure.

The second concept, shown in Figure 6b, studied is the mini-channel cold plate concept applied to a full battery module with coolant flowing in between each pair of cells, through the units, and ultimately the entire module. This concept provides better thermal performance through reducing the total thermal resistance by eliminating a layer of TIM and the fins from the pack construction. The structure of the battery module then becomes the mini channels that route the coolant throughout and will be investigated as a potential improvement from the baseline flow configuration case.

Finally, a newer concept can be investigated due to the improved and expanded module construction which is a distributed flow (DF) concept, shown in Figure 6c, where the cooling channel runs across the battery cell length and is then ducted to return across adjacent battery cells. The theory behind this design is that the distribution of cooling throughout the module will lead to lower pack temperature distributions at the same flow conditions as the SC concept.

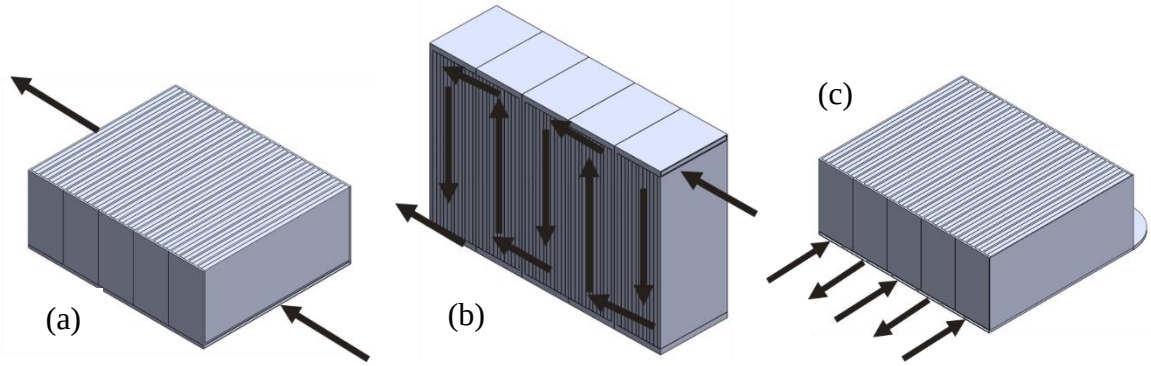

Figure 6: (a) Straight channel (SC), (b) Interflow (IF), (c) and Distributed flow (DF) configuration

3.4.3 Battery Coolant Flow and TIM Study Methodology

The battery coolant flow study is divided into three separate studies: flow study optimization and characterization, TIM performance study, and the dynamic coupling of COMSOL module-level results to Modelica transient simulations. The flow and TIM study share similar boundary and simulation conditions which are outlined in this section.

Beginning with the boundary conditions derived from the transient model, these are the maximum flow rate ($0.25 \cdot 10^{-3}$ m^3/s) range of inlet temperatures (293 K to 303 K), battery configuration (5s 8p), max rated current which will be doubled for a theorized safety factor (0.75 C), and finally battery cell dimensions which are modified to a more optimal aspect ratio of 2.1 [59] to maintain relevance with current manufacturer trends. Additionally, the upper limit of thermal contact conductance is taken to be $300 \cdot 10^{-6}$ m^2-K/W [60].

For the first study on flow orientation, three variables will be considered in the parametric study: flow rate, inlet temperature, and module configuration itself. The outputs will be max cell and pack temperature, cell and module temperature difference, pressure difference across the cold plate solution, and thermal resistances for the cold plate defined based on difference between the battery max temperature and coolant inlet temperature as its input. The second study on TIM performance seeks to examine trends in the above outputs as a function of parameterized TIM contact conductance as well as flow orientation. These studies are summarized in Table 7. Fractional values indicate that the maximum of flow rate or TIM performance established is varied as a fraction of the maximum amount at that test condition.

Table 7: Flow and TIM study parametric table of simulations

$\dot{V}_{flow} \backslash T_{inlet}$	25	30	35	$TIM_{Fin} \backslash TIM_{Gap}$	1/3	2/3	1
1/3	✓	✓	✓	1/3	✓	✓	✓
2/3	✓	✓	✓	2/3	✓	✓	✓
1	✓	✓	✓	1	✓	✓	✓

The numerical framework for both sets of studies is COMSOL Multiphysics 5.5 with modules for electric circuit parameterizations, laminar flow, and heat transfer. The flow and heat transfer

models are coupled via non-isothermal flow to fully parameterize the packs behavior. Battery parameters identified for the Modelica battery model are used to fix heat rejection from each cell which is uniformly generated throughout each cell at its own specific reference conditions. In this way, each cell is discretized as its own independent heat source dependent on average cell temperature and pack state of charge. These are steady state simulations with the identified boundary conditions with electrical, flow, and heat transfer domains are solved at each step of COMSOL's solver at preset grid densities of coarser for each domain. Further information on grid independence studies is identified in the appendix in Figures A1 and A2. This concludes the COMSOL modeling methodology leaving only the coupling to the Modelica environment left to define.

3.4.4 COMSOL and Modelica Coupling Methodology

With the modeling methodology established for COMSOL simulations, these results must be coupled to the transient environment of Modelica to enable a closed feedback loop of battery module performance on transient system control and EV design. This coupling takes the form of generated lookup tables parameterizing module level performance as a function of volumetric flowrate. These lookup tables are imported into the Modelica environment and used in parallel and series flow relations to establish the total pack resistance as a function of battery pack flow orientation and module level performance. An added caloric resistance term is considered with the addition of modules in series while the coolant flow is split evenly between the number of parameterized parallel modules. The module, defined previously as 5s and 8p, has a total of 40 cells. To achieve the theoretical performance established in the ITMS Modelica model and additional 21 modules are needed, in any series or parallel flow orientation, to achieve necessary battery pack capacity. In this way there are again three variables identified for study: number of cells in parallel, series, and the flow orientation utilized (either SC, DF, or IF).

4. RESULTS

With the modeling methodology, thermal system architectures, and boundary conditions established, the six thermal management systems are simulated across the MCT cycle. This allows for comparisons of driving range across parameters of the thermal management system, ambient temperature, and cabin setpoint temperature. A transient cycle for the WHR system of most interest is examined across a MCT simulation, highlighting the heat transfer and control setpoints during transient performance. After the determination of an optimal thermal management system for long range electric vehicles, the identified cycle is used as a boundary condition for a battery coolant flow study investigating flow orientation, pack construction and TIM performance, and the coupling of COMSOL results with the Modelica transient modeling environment.

4.1 ITMS Results

The results of the ITMS simulations are split between final range comparisons of each systems across ambient temperature and cabin setpoints, and the transient results of the optimal thermal management system for long range BEV's, the WHR system.

4.1.1 ITMS Range Comparison

The bar charts presented in Figure 5 show the system ranges across the range of ambient temperatures at each cabin setpoint temperature. Battery trials are excluded as their results had little impact on overall system range varying the overall range approximately 2% across the investigated range of battery variation. Clear trends are observed in system performance as the cabin setpoint varies across the range of ambient temperatures. On average, for each architecture in most stringent cooling mode (i.e., ambient of 40 °C). the projected range for the system decreases by ~2-3% for every 2 °C reduction in the cabin setpoint from 24 °C to 18 °C. This leads to an overall variation of 12% in driving range for the baseline system depending on the user-determined cabin set point. These cycles have the same cooling performance, except the LT HX system, because all their assumed components and control behavior are identical in cooling mode.

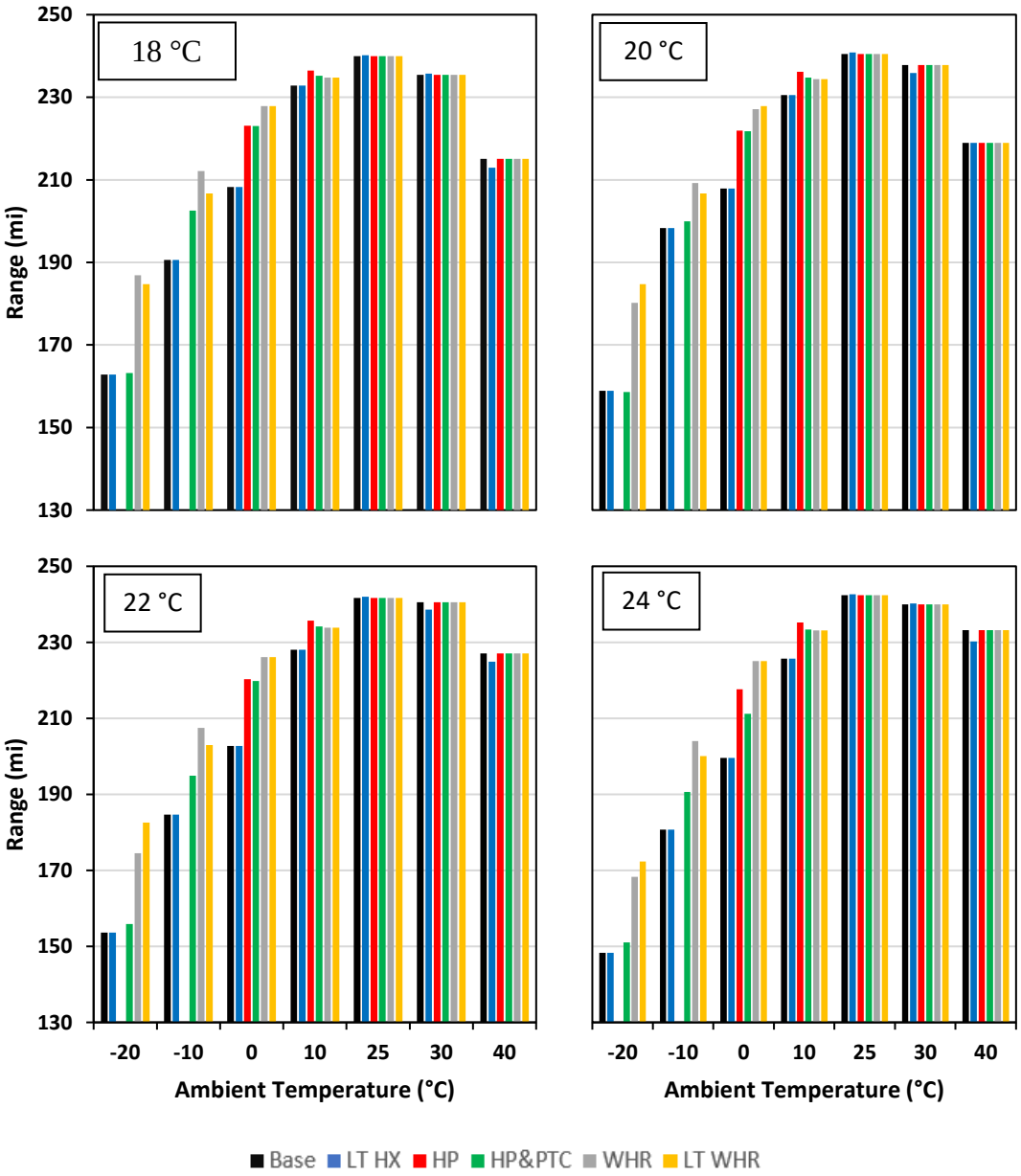

Figure 7: Simulated driving ranges for each ITMS architecture (Base, LT HX, HP, HP&PTC, WHR, and LT WHR) across a parametric variation in ambient temperature (-20 °C, -10 °C, 0 °C, 10 °C, 25 °C, and 30 °C) at cabin setpoints of: a. 18 °C, b. 20 °C, c. 22 °C, and d. 24 °C.

The LT HX system was theorized to provide low temperature cooling for the battery, but compared to the baseline, provides only a very slight benefits at the 25 °C ambient condition, while showing no benefit at the other test conditions. This radiator, while implemented to provide low temperature cooling of the battery, was observed to only provide benefit in a mixed heating and cooling condition, namely, when the cabin requires marginal heating while the battery would

require cooling. The range of ambient conditions tested does not provide any opportunities for this necessary mixed condition where cabin conditioning would be negligible and the battery could be cooled with a relatively cool ambient. Future work could examine a mix of moderate test conditions to examine mixed system use-cases that might highlight the benefits of this system.

Under the ambient temperature range that demands cabin heating (from -20 °C to 10 °C), the system architectures become more distinct in their performance. Compared to the cooling demands, these heating cases having more severe impact on driving range that justifies a focus on exploring architecture improvements for heating efficiency. Beginning with a general assessment, an overall decrease in the max range of 32.9% to 38.9%, depending on the cabin setpoint temperature, is experienced by the baseline system as the ambient temperature is reduced to -20 °C. This amounts to a total range reduction of 80 to 100 miles for the baseline system. Examining the heat pump architecture (HP), improved performance relative to the baseline is observed at ambient temperatures ranging from 0 °C to 10 °C, but the heating performance is inadequate to meet the heating demand at -20 °C and -10 °C (bars therefore not shown for these unviable operating points). There are several potential solutions to this issue with the HP system. Active control of the recirculation ratio could decrease the ventilation loading and allow for adequate heating of the cabin down to low ambient temperatures of -20 °C; however, this would risk fogging of the windshield and pose a hazard to driver safety. Alternatively, the compressor size (which was sized for the baseline system cooling load) could be increased to provide the necessary capacity at lower ambient temperatures, with the tradeoffs being additional cost, size, and weight of the VCC components. Finally, the addition of an electric heater to compensate for lack of capacity is the most practical solution, and the basis for the HP&PTC architecture. This HP&PTC architecture maintain the performance gains of the HP system relative to the baseline at ambient temperatures of 0 °C to 10 °C. More critically, the addition of the PTC heater makes up any heating capacity shortfalls of the heat pump system, but compared to the baseline, the continued operation of the compressor at low temperature benefits the system it can provide heating with a COP > 1. Ultimately, this HP&PTC architecture can achieve the cabin setpoints at -20 °C (with little range benefit) and provides a measurable range increase of ~5% over the baseline system at -10 °C. This extends the use of a traditional HP scheme to a lower temperature bound nd maintains the HP performance improvements at moderate temperatures of 0 °C to 10 °C with this simple addition of a four-way valve (V4).

With the baseline use of water glycol loops for cabin and battery conditioning, the WHR architecture was established to allow heat scavenging from the electronics cooling loop. The WHR system mirrors the range performance of the HP&PTC system at moderate ambient temperatures but provides clear advantages at lower ambient temperatures (0 °C to -20 °C). At these temperatures, the system experiences a further increase in effective range owing to the utilization of waste heat. At the 0 °C ambient condition, only a moderate increase of 3% in driving range is gained as compared to the HP&PTC system because the system load can still be met with the compressor. But at the -10 °C and -20 °C test conditions, the compressor cannot provide all the heating load necessary for the cabin in the HP&PTC system. At these ambient temperatures, the WHR system can supplement the necessary cabin heating requirements, which leads to the relative increase in range as compared to the HP&PTC system. This increase is large at the -20 °C condition as a larger portion of electric heating is needed to meet the demand in the HP&PTC system compared to the WHR system. The next section will further discuss the transient response of the WHR system to illustrate the reduced electric heating load due to recovered heat from the power electronics.

Further improvements to the extreme low temperature performance motivated the analysis of the LT-WHR architecture. With the addition of the low temperature battery radiator in this system, the results at -20 °C ambient are investigated and compared to the WHR system to determine if the LT waste heat utilized by the LT WHR system provides a significant benefit to system range. As observed in Figure 7, this depends upon the cabin setpoint temperature. At -20 °C, with a cabin setpoint of 20 °C to 24 °C the LT-WHR system provides an appreciable increase in system range of 2% compared to the WHR architecture. At an 18 °C cabin setpoint and -20 °C ambient there appears to a penalty imposed by this system. This is due to oscillation of the electric PTC heater as it nears its shutoff condition. This prolongs the use of this heater and causes the decrease in range observed. This performance benefit observed at setpoints of 20 °C to 24 °C cabin setpoints disappears however at any higher ambient temperatures because the recovered heat from the power electronics is sufficient to supplement the steady state electric heating requirements of the system. The addition of the low temperature radiator in the LT-WHR system has no performance benefit as the offset compressor power is already negligible at this point. Overall, the implementation of this LT-WHR system, while it provides for increased system

range at extremely low ambient temperatures, provides little overall benefit for the increase in complexity and necessary system components.

Considering the tradeoffs in system complexity versus range benefits over a wide range of typical ambient and cabin temperature, the WHR system seems to be optimal ITMS for long range electric vehicles among the architectures compared in this study. A logical extension of this modeling work is an addition to the modeling framework for technoeconomic investigation of the systems to quantify their range extension in terms of added system components and complexity. This could allow broad comparison of the technoeconomic tradeoffs between candidate EV thermal systems.

4.1.2 ITMS Transient Control

Shown in Figure 8 is a plot of the transient compressor power, PTC heater power, and cabin HX throughout the drive cycle for the WHR architecture simulated at an ambient temperature of -10 °C, a cabin setpoint of 24 °C, and a battery setpoint of 15 °C. Several features of the control logic are illustrated in this plot. First, from the initialized soak condition, the electric heater for the cabin is set to a maximum of 6 kW of power, in contrast with that of the HP&PTC architecture that necessitated an 8 kW maximum (not shown). This is due to the added waste heat in the system as well as the battery and cabin heater being placed in line with each other, allowing them to work together in heating operation. A clear gap in heating performance is observed between 0 s and when the cabin then reaches its setpoint at ~1400 s. The 6 kW of power for the electric heater appears to not be transferred to the cabin HX. This is due to the orientation and layout of the flow control systems in the WHR architecture, the thermal mass of the battery, and the size of the battery heater itself. Its observed from Figure 4e that the cabin PTC heater flows into the battery which extracts heat before the cabin HX, effectively delaying the heating action of the cabin which can be seen completes at 1400 s in the transient plot, at which point the PTC heater begins to adjust to control the inlet cabin temperature while the system actuates the inlet volume flow rate. A corresponding dip in battery heating can be observed. In this way, the sizing of the battery heater, the orientation of the flow systems, and the battery thermal mass can have significant deleterious effects on the cabin heating performance which are clearly demonstrated.

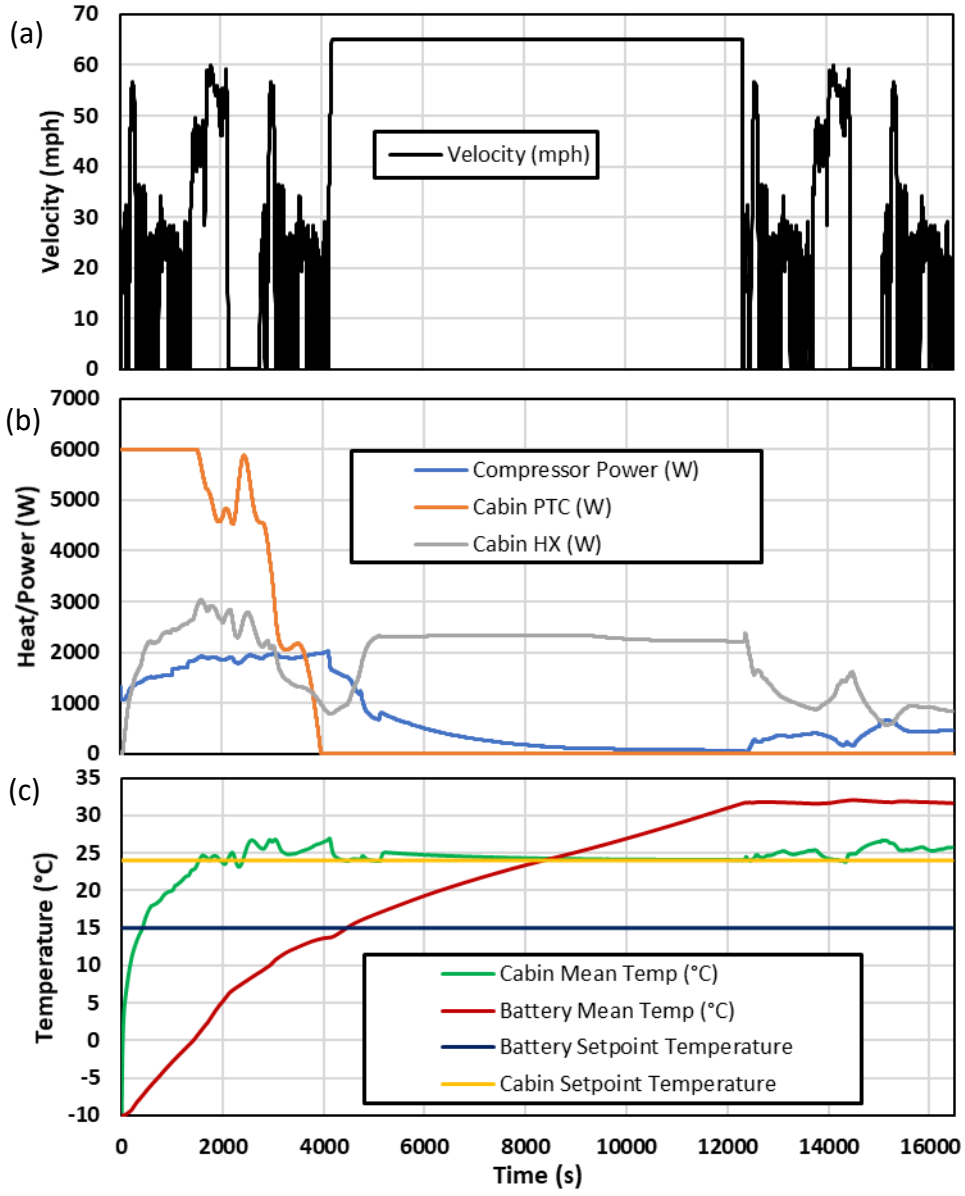

Figure 8: (a) simulated MCT drive cycle. The simulated heat loads and power draws throughout the cycle time are plotted for: (b) the heat exchange in the WHR architecture at -10 °C ambient with a 24 °C cabin and 15 °C battery setpoints; and (c) the setpoints of the WHR architecture at -20 °C ambient with a 24 °C cabin and 15 °C battery setpoints

At this point, from 1700 s to 2600 s, the flow rate into the system initially decreases as the cabin setpoint is surpassed and, due to slight fluctuations in PI control, dips briefly below its setpoint until settling at the control point as the fan volume flow rate decreases. Eventually, at ~4000 s, the electric heater completely shuts off while the cabin HX and compressor power completely compensate for the necessary steady state heating load of the system. As time

progresses, during the high constant speed portion of the cycle, the WHR supplements most of the heating load, allowing the compressor to essentially shut off. After this constant speed portion, at ~12000 s, the system enters a mixed control condition where the compressor controls the cabin inlet temperature while the power electronics radiator is completely bypassed. Overall, this control scheme and architecture meets the necessary EV setpoint temperatures while extending system range via the utilization of waste heat. Compared to the baseline, this flow control is enabled through the addition of a four-way valve (V4) to allow operation of the VCC as a heat pump and two four-way valves (V5 and V6) actuated to allow waste heat recovery. Implications on future work and system implementation are clear, as this result demonstrates the need for study on effective and flexible flow configuration, as well as the benefits of battery and cabin pre-heating.

4.2 Battery Coolant Flow Study Results

The results of the flow study are split into three segments, the flow optimization, TIM study, and coupling to Modelica modeling environment to demonstrate the coupled nature of module design with overall pack performance.

4.2.1 Battery Coolant Flow Optimization

Beginning with an overview of the results, Figure 9 summarizes each flow orientation across the parameteric study of battery module inlet temperature and flow rate. Some immediate conclusions can be draw, the first being that the IF design has the best thermal performance. . Second, the SC module has the lowest pressure drop, which is to be expected as it has the simplest flow orientation. The IF module has pressure drops 5 times larger than the SC module. The DF module additionally has higher pressure drop than the IF, approximatley 200 Pa . This increased pressure drop for the DF flow orientation is likely due to effects of ducting coolant back across the battery module. This is a fair comparison, however, as the DF model relies on this recirculation of coolant in its theorized performance benefit over the SC model.

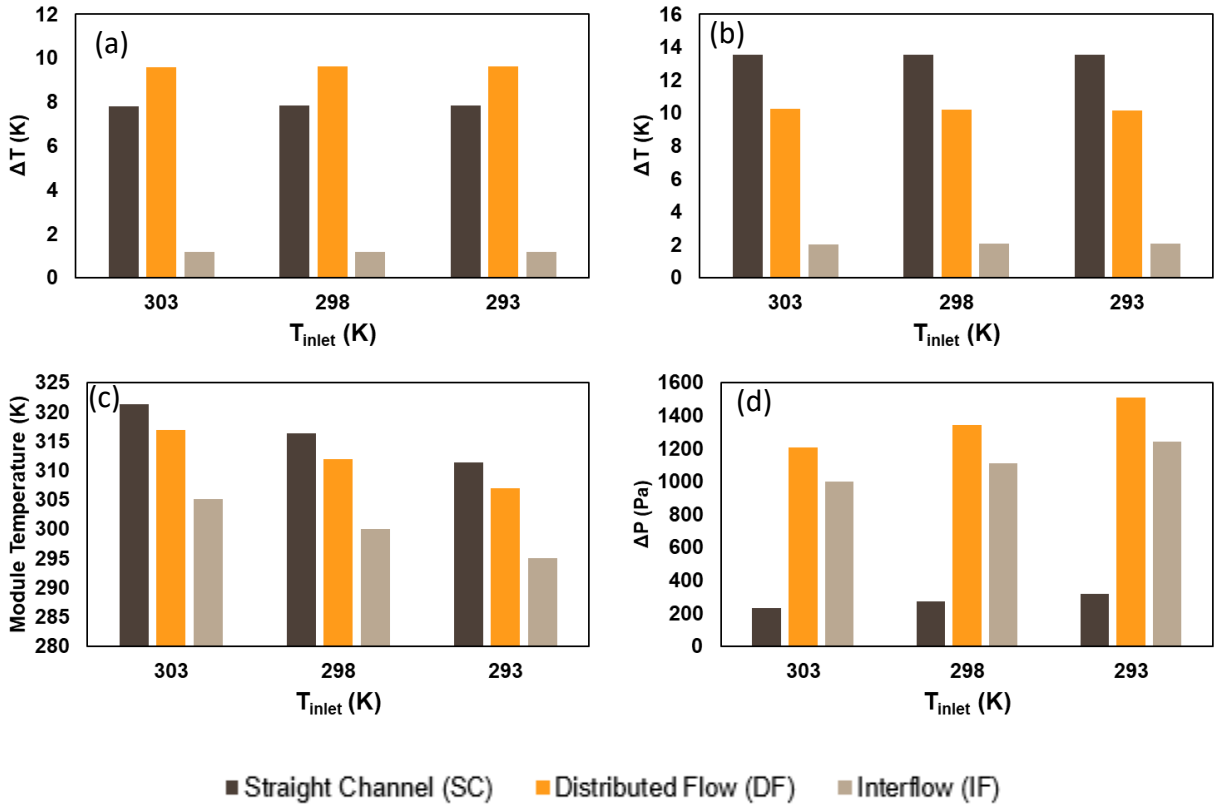

Figure 9: Results of flow configuration study for (a) cell temperature difference, (b) module temperature difference, (c) module max temperature, and (d) module pressure difference

With the IF orientation established having the best thermal performance, the SC and DF orientations are more directly compared across the simulation range. This is shown in Figure 10 to Figure 12. Beginning with cell temperature difference ,the SC module provides for a lower cell temperature difference than the DF as shown in Figure 10. This is due to the SC module cooling across the thickness of the battery cell, while the DF module cools across the length of the cell. This difference is ~2 °C at maximum and worth noting as cell temperature difference is a key metric for cell longevity and health.

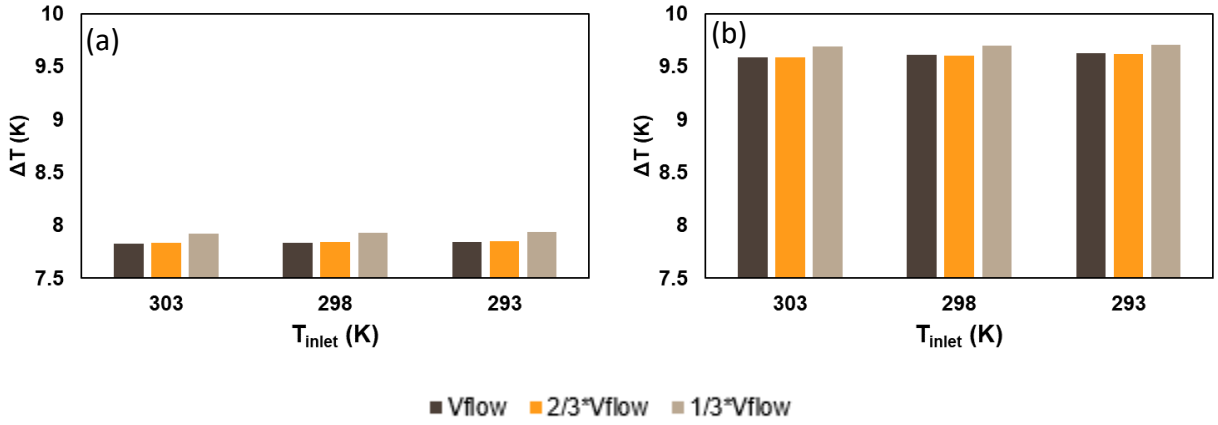

Figure 10: Comparison of (a) SC Cell Temperature Difference vs (b) DF Cell Temperature Difference

Examining next the module temperature difference, three key conclusions can be drawn. First, the DF module, shown in Figure 11b, has at maximum an overall 5 °C decrease in module temperature difference as compared to the SC module. Additionally, the DF module temperature difference decreases with decreasing flowrate while the SC module temperature difference increases with decreasing flowrate. As flow rate decreases, the coolant temperature increases more along the cold plate in both modules. In the case of the SC module, thermal mass at the end of the battery pack has no thermal communication with the cooler sections of the battery pack at the inlet and thus cannot distribute heat effectively throughout. The DF module is meant to address this with the cooler sections and the cold plate inlet interfacing directly with the hotter sections at the outlet.

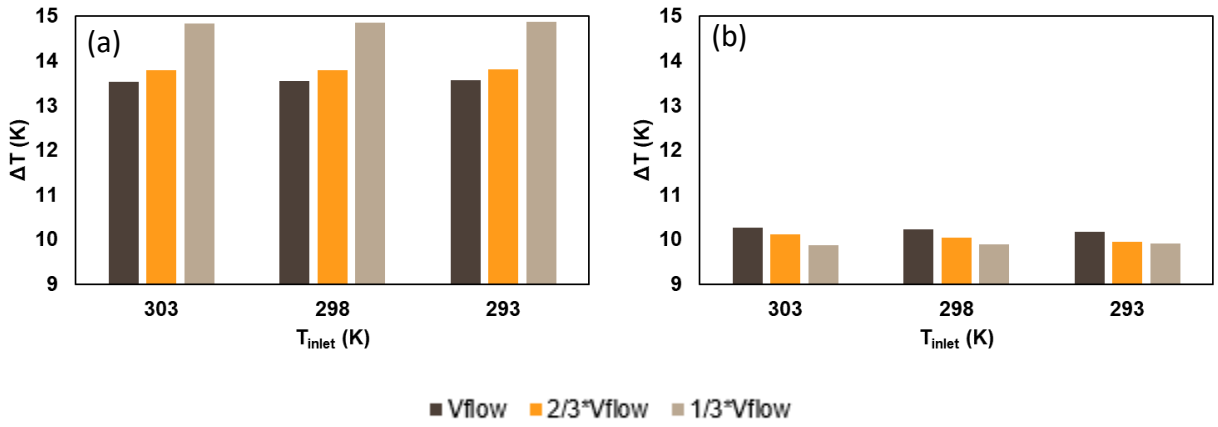

Figure 11: Comparison of (a) SC Module Temperature Difference vs (b) DF Module Temperature Difference

The final comparison between the SC and DF modules comes in the form of max module temperature, shown in Figure 12. Similar conclusions can be drawn here with the dependence of module max temperature on flow rate decreased, from a 5 °C increase to a 3 °C increase, and the overall max temperature of the module decreased on the order of six degrees overall. This result confirms the original purposes of the DF module, namely, the utilization of battery thermal mass to reduce temperature difference and max module temperatures. These gains in module cooling performance come at the expense of additional system pressure drop. Additionally, confirms the benefits of modeling the battery module with increased resolution on pack construction and TIM placement.

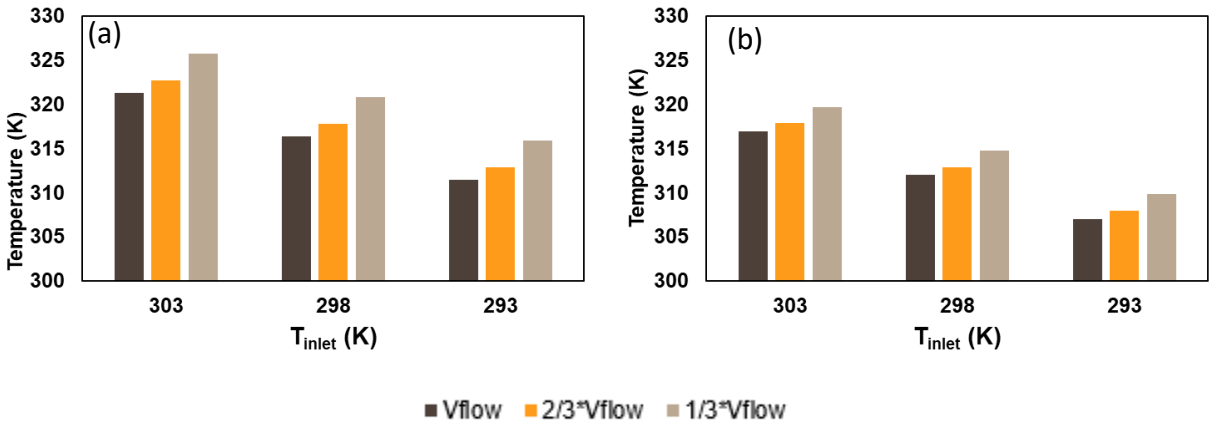

Figure 12: Comparison of (a) SC Max Module Temperature vs (b) DF Max Module Temperature

4.2.2 Battery TIM Study

To study the effect of TIM performance, each module was simulated across the parametric Table 7 . The trends in the results were the same across all flow configurations, and for brevity a single orientation, the DF model, is presented in Figure 13. In Figure 13a as Gap TIM resistance increases cell temperature difference decreases on the order of a degree. This is because as the thermal pathway between the battery, fin, and cold plate poses a higher resistance and heat is distributed more uniformly throughout the thermal mass of the battery. The opposite can be observed with the Fin TIM contact resistance. As Fin TIM contact resistance increases, pathways for heat flow inside the pack pose a higher resistance, reducing thermal spread inside of the pack and temperature differences increase. As a for a consequence decreasing Gap TIM thermal resistance and thus improving cell and module temperature differences, battery pack max temperature increases up to 2 °C and module level thermal resistance increases 10% as shown in Figure 13c and Figure 13d. These results demonstrate the importance of TIM parameterization to module level thermal performance and are adopted as an input to transient modeling going forward.

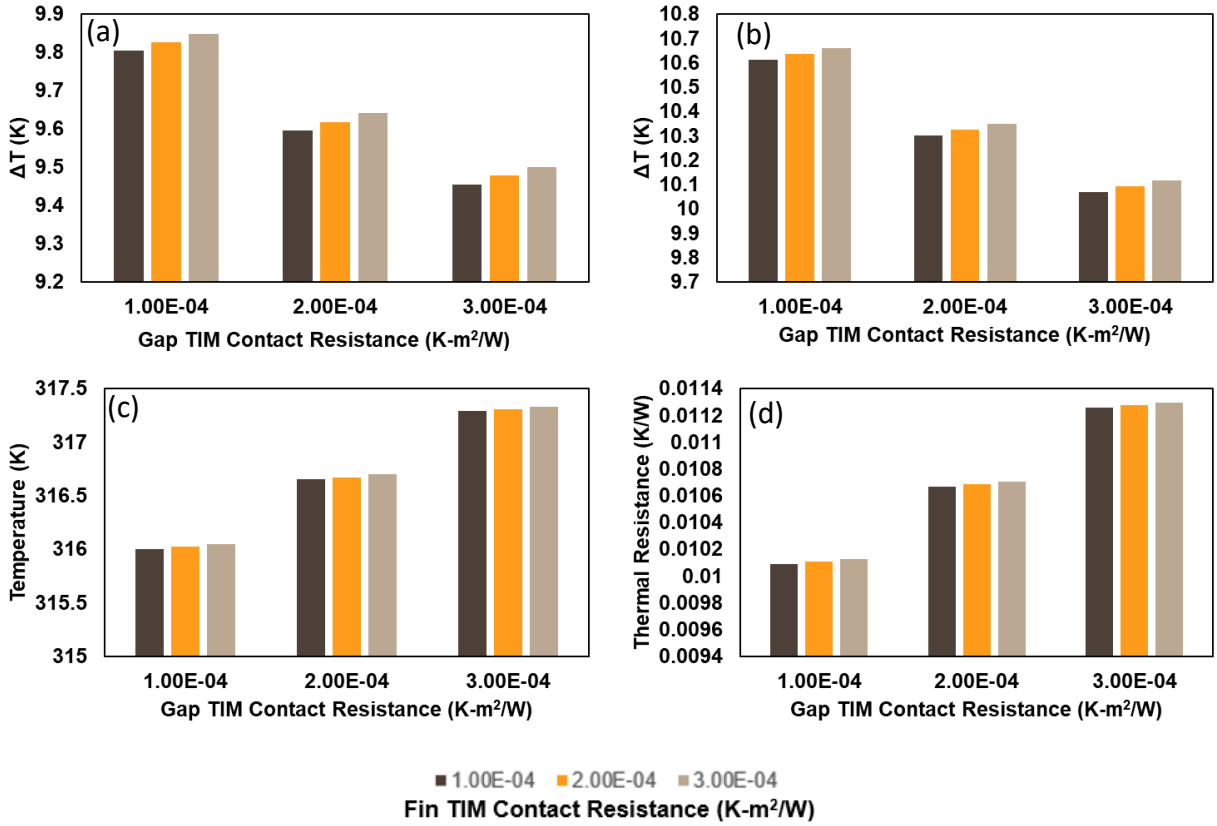

Figure 13: Results of TIM study comparing influence of contact conductance of TIM's on the cold plate (CP) vs those on the battery cells on (a) cell temperature difference, (b) module temperature difference, (c)module max temperature, (d) and module thermal resistance

4.2.3 Coupling Modelica to COMSOL Simulations

Finally, with module-level cooling solutions studied the lookup tables necessary for integration with the transient Modelica environment can be generated. A single case study for cooling performance is studied at a 40 °C ambient condition with battery and cabin setpoints of 24 °C and 18 °C, respectively. This cooling case is designed to show distinction between module level cooling solutions as a function of the parameterized flow orientation inside of the module and flow orientation at the battery pack level. The baseline cooling solution, the SC orientation, is studied in a 21S and 1P battery pack flow configuration. This result is shown in Figure 14a with the battery initially struggling to be cooled to its setpoint under transient heating load. At the point where the CSC cycle begins, about 4000 s, the battery temperature evolves past its limits up to a max temperature of approximately 45 °C until the heating load decreases again at 12000 s. This demonstrates that under high loading, the added caloric resistance from the flow configuration dominates the battery pack thermal performance and causes inadequate cooling under high CSC loads. As a contrast, the IF design with a battery pack flow configuration of 3S and 7P is studied in Figure 14b. After adjustment of the maximum flowrate inside of the battery coolant loop, the IF module effectively cools the EV battery under all conditions throughout the cycle demonstrating both the improved thermal performance at the module level but also the reduction of additional caloric resistance due to active management of pump speed. This is shown in Figure 15 with the pump mass flow rate graphed against the total thermal resistance of the EV battery pack showing its responsiveness to system control logic and setpoints throughout.

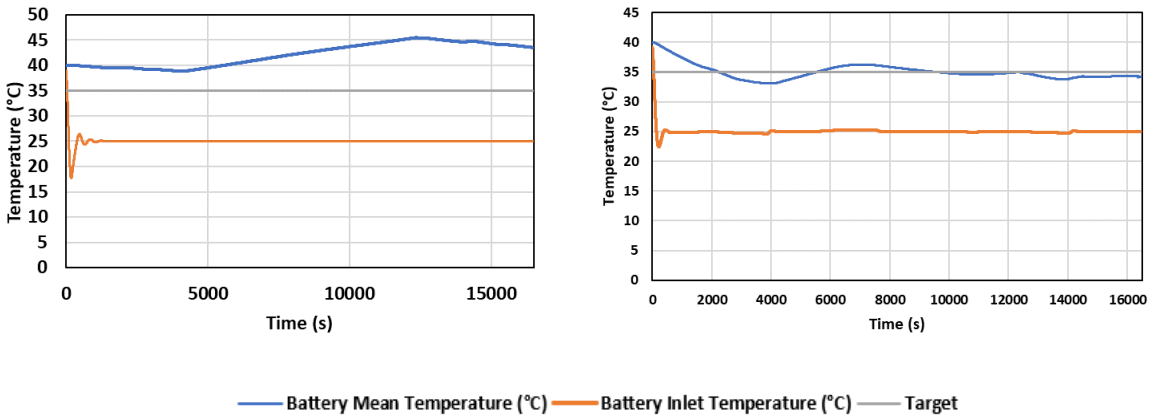

Figure 14: Results of module level coupling of module thermal resistance to dynamic modeling for (a) SC flow orientation with 21S and 1P vs (b) IF orientation with 3S and 7P

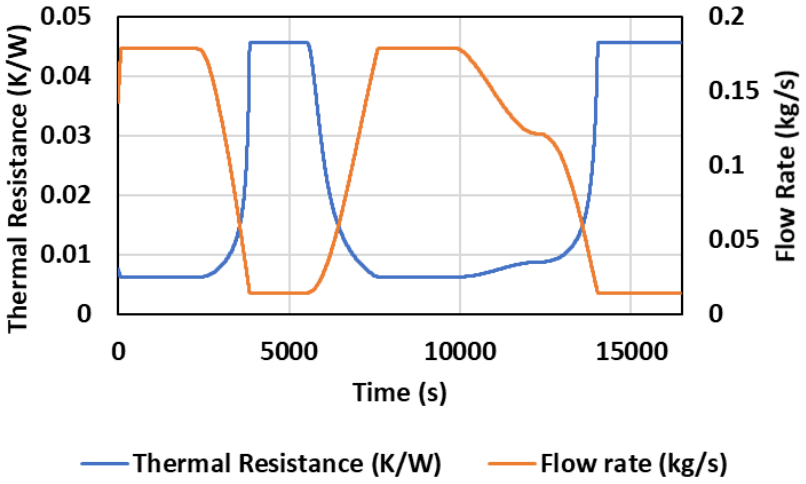

Figure 15: Thermal Resistance vs Time and Flow Rate vs Time for the IF 3S 7P battery pack orientation

5. DISCUSSION AND CONCLUSIONS

This work performed a comparative investigation of integrated thermal management systems (ITMS) for long-range battery electric vehicles, using a comprehensive dynamic model to evaluate the range performance across various thermal systems architectures. This is completed for traditional thermal management systems commonly studied in open literature as well as a novel solution defined for this work. This approach unifies results that were previously scattered across a wide range of boundary conditions, vehicle drive schedules, and user-defined control parameters, hampering a direct comparative analysis. The impacts on range of cabin thermal management are clearly enumerated with the impacts of the large thermal masses of the battery and cabin quantified in a transient simulation of mixed control schemes. These have broad implications for the optimal thermal management system for long-range EV's. Moving then to the battery coolant flow study, three flow configurations are studied with boundary conditions adopted from the established dynamic modeling framework. These concepts (SC, DF, and IF) are then compared against each other in terms of thermal and pressure drop performance. The pack construction is then studied, rating the influence of TIM contact resistance at the gap pad and fin location. Finally, the module-level results are coupled to the transient ITMS model previously established and the effects of battery pack flow configuration, added caloric and module level resistance, and their effects on the cooldown time across a dynamic MCT cycle is studied.

Several key conclusions are drawn regarding long-range BEV thermal system performance and module level cooling studies of EV batteries:

1. From the HP&PTC architecture, the extension of system heating performance with a PTC heater can yield extended range above the baseline system even at extremely low ambient temperatures.
2. The inclusion of the battery as a necessary heating mass places a burden upon combined WHR systems that require further system optimization.
3. The advantages of the WHR system is further shown when examining the components necessary to enable its advantages; namely only the addition of three four-way, flow reversing valves and the use of a common heat transfer fluid, water glycol.

4. The novel LT WHR system defined in this work, provides some performance benefit compared to a WHR system but not enough to justify the additional equipment and control structures necessary.
5. A comprehensive review of battery circuit modeling is conducted with the perspective of integration of open-source data with flexible modeling platforms. It was concluded that usable, temperature-based, ECM's are rare in literature.
6. WHR systems provide unique benefits for these long-range systems depending on the drive schedule enabled by their long-range operation.
7. The interflow module design provides next generation conditioning for battery packs at the risk of additional leaks and more involved pack construction and flow routing.
8. The DF concept studied provides better thermal performance than traditional SC concept at the expense of additional pressure drop and additional cold plate construction.
9. Module max temperature can vary up to 2 ℃ while increasing module and cell temperature difference by improving TIM performance inside of battery modules, demonstrating the need for enhanced construction inside battery pack simulations.
10. Finally, the coupling of module level COMSOL results to the Modelica transient environment is complete, demonstrating the impact of battery pack flow construction, added caloric resistance, and the impact of module level performance on EV transient cooling control.

Natural extensions of this work could be the adoption of additional novel thermal management systems such as direct two-phase cooling of the battery, investigations into gain scheduling, battery, and cabin pre-heating control schemes, and charging scenarios and associated battery thermal management.

APPENDIX

Table A1. Battery cell parameters

Parameter	Value	Unit	Source
Capacity (Electric)	31	Ah	[35]
Capacity (Heat)	810	$J/(m^3K)$	[35]
Length	0.215	m	[35]
Thickness	0.0084	m	[35]
Height	0.22	m	[35]

Table A2. Battery pack parameters

Parameter	Number
Cells (Total)	840
Cells (Parallel)	8
Cells (Series)	105

Table A3. VCC and electronics radiator dimensions

Parameter	Value	Unit
A_o	4	m^2
A_i	0.464	m^2
Length	0.418	m
Depth	0.012	m
Height	0.565	m

Table A4. Cabin evaporator dimensions

Parameter	Value	Unit
A_o	2	m^2
A_i	0.755	m^2
Length	0.249	m
Depth	0.023	m
Height	0.249	m

Table A5. Cabin heater core dimensions

Parameter	Value	Unit
A_o	3.38	m^2
A_i	0.339	m^2
Length	0.249	m
Thickness	0.132	m
Height	0.254	m

Table A6. Battery evaporator (plate HX) dimensions

Parameter	Value	Unit
A	0.464	m^2
Plates	40	-
Length	0.0508	m
Width	0.1524	m

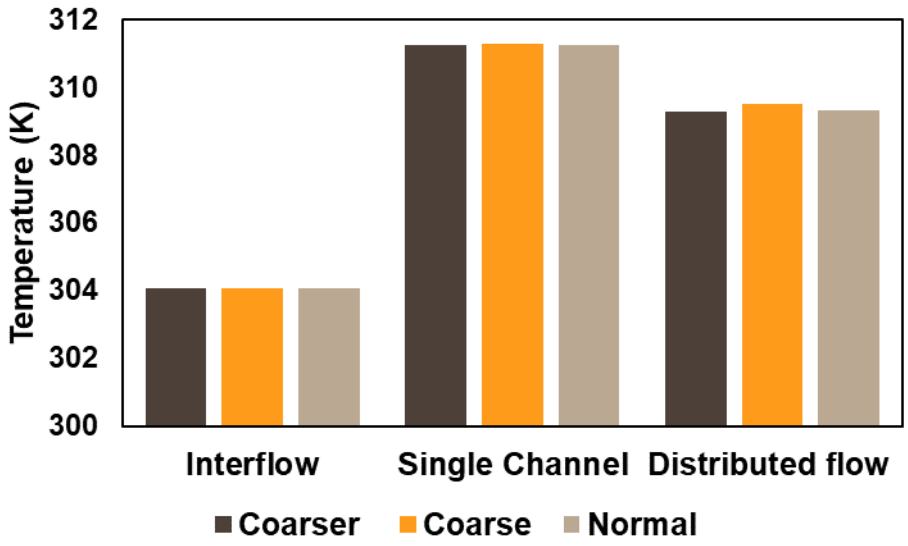

Figure A1: Grid independence study for identified flow configurations

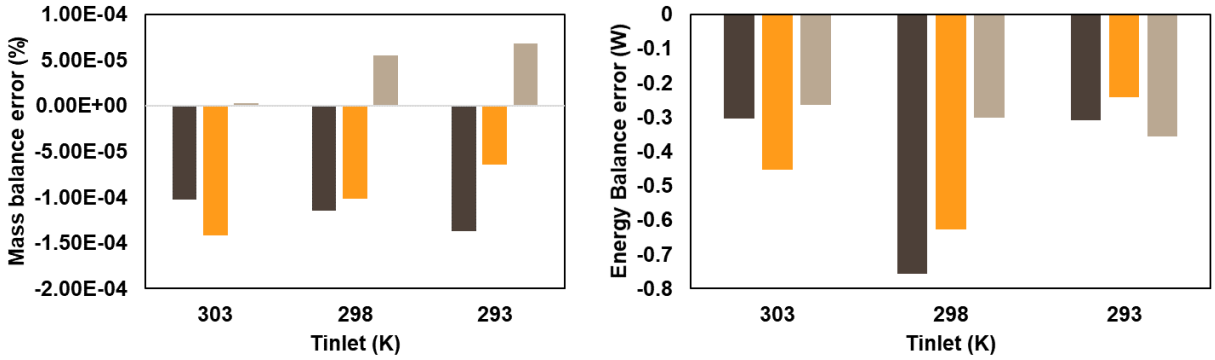

Figure A2. (a) Mass balance error (%) and (b) energy balance error (W)

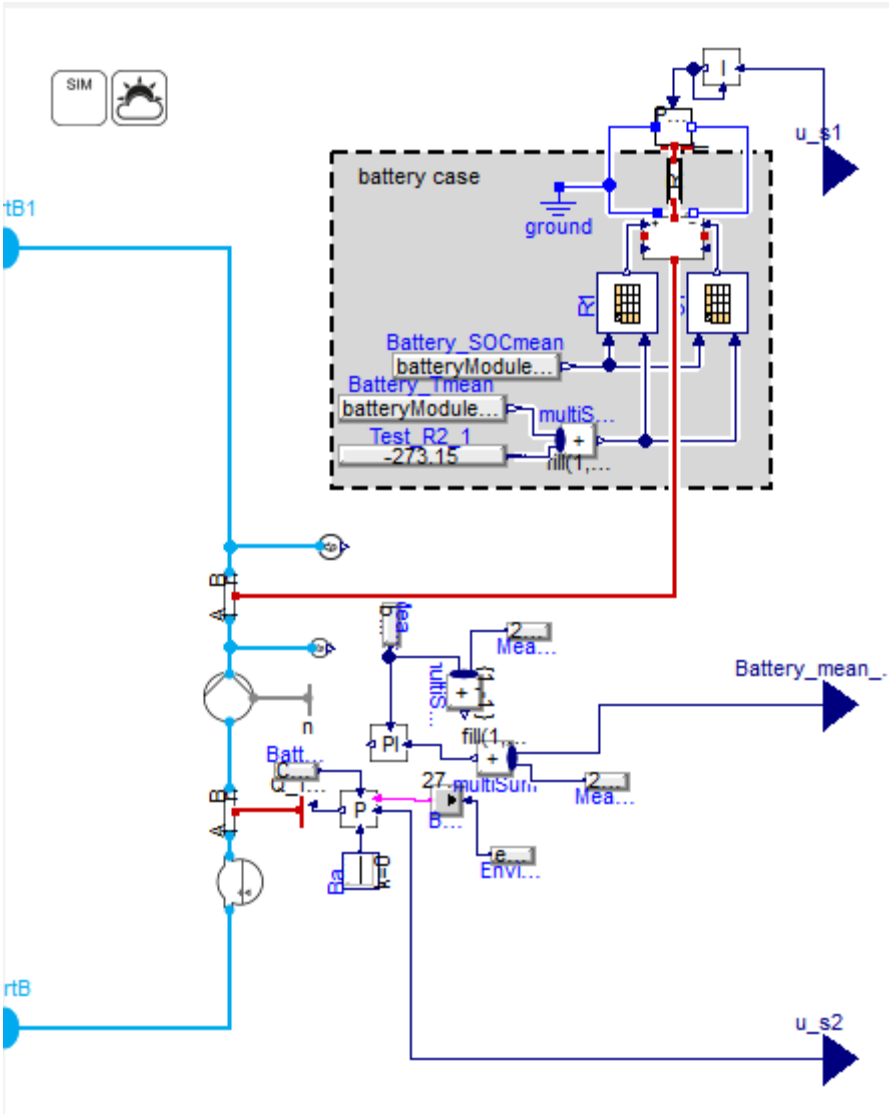

Figure A3: Typical battery sub-model in Modelica environment

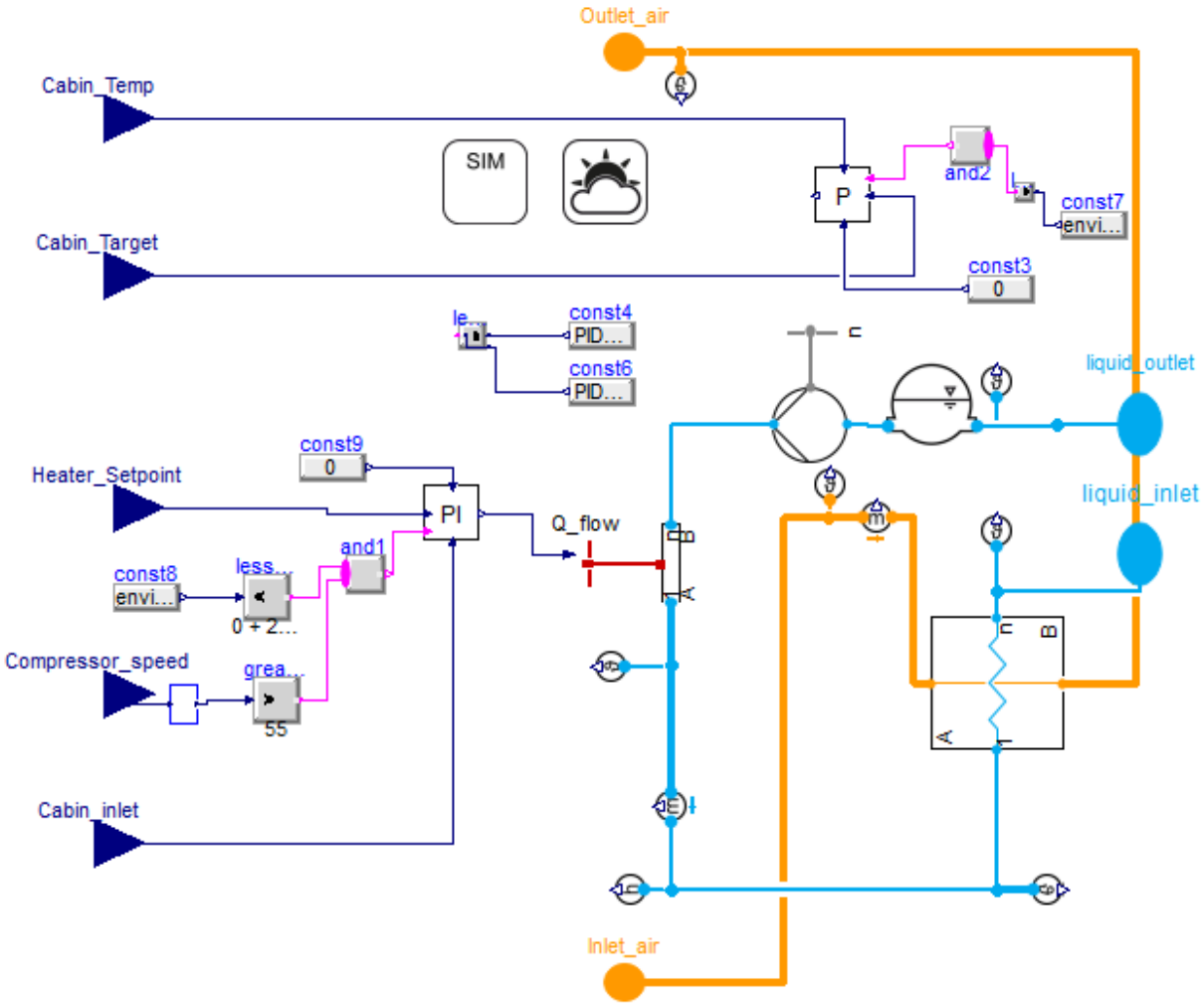

Figure A4: Cabin heating sub-model in Modelica environment

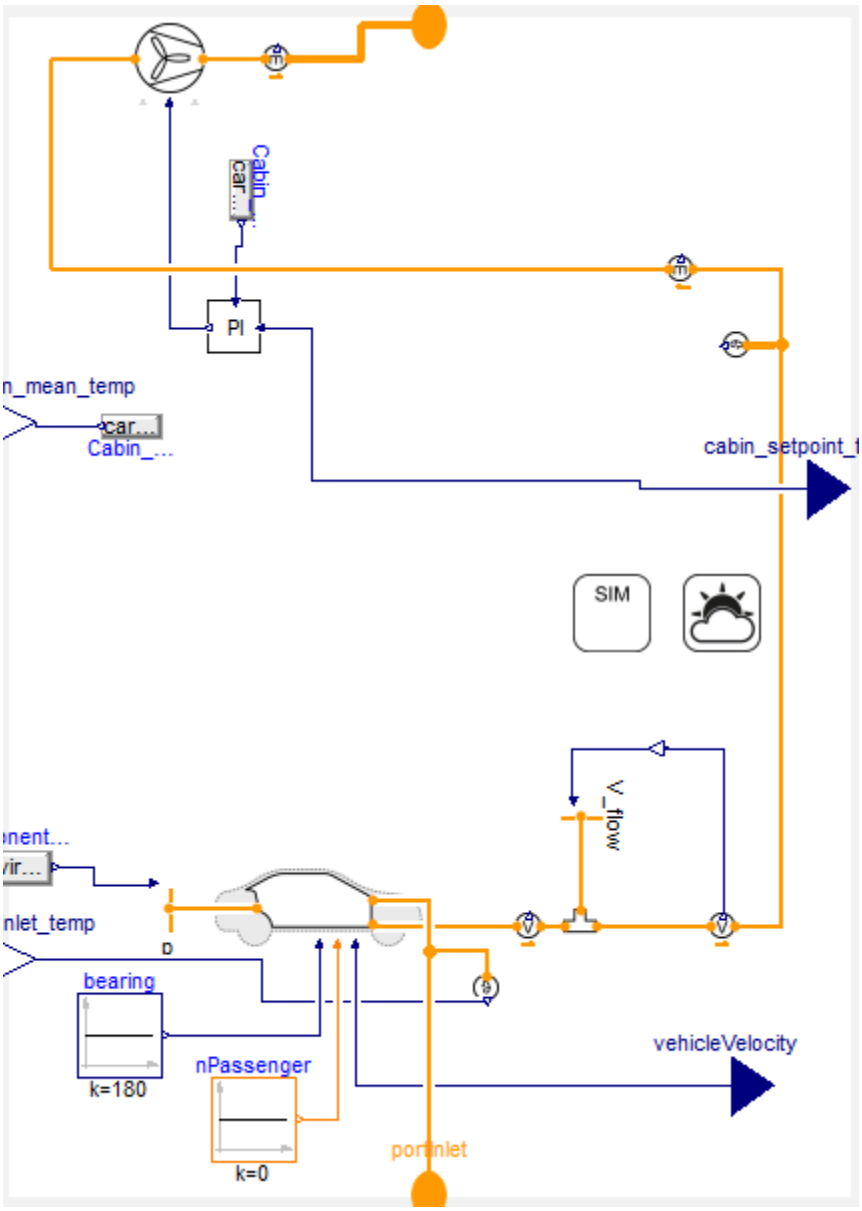

Figure A5: Cabin HVAC sub-model in Modelica environment

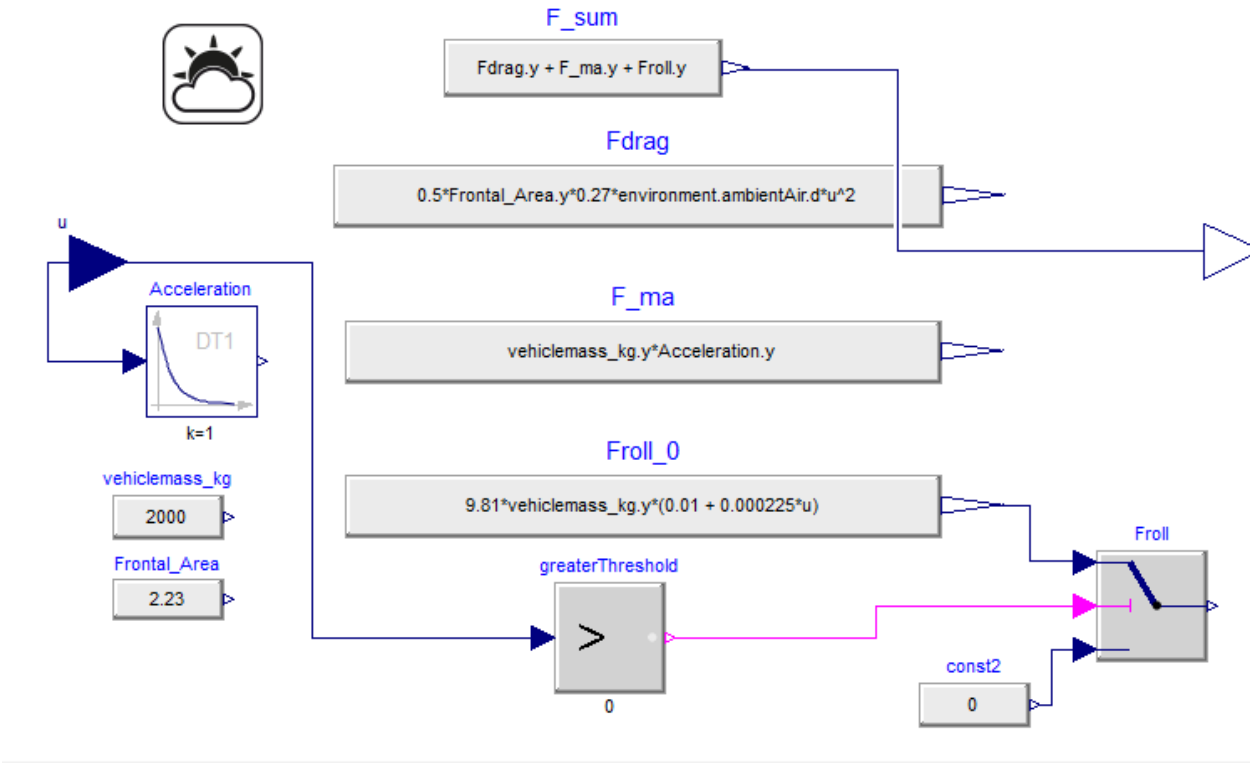

Figure A6: Drivetrain sub-model in Modelica environment

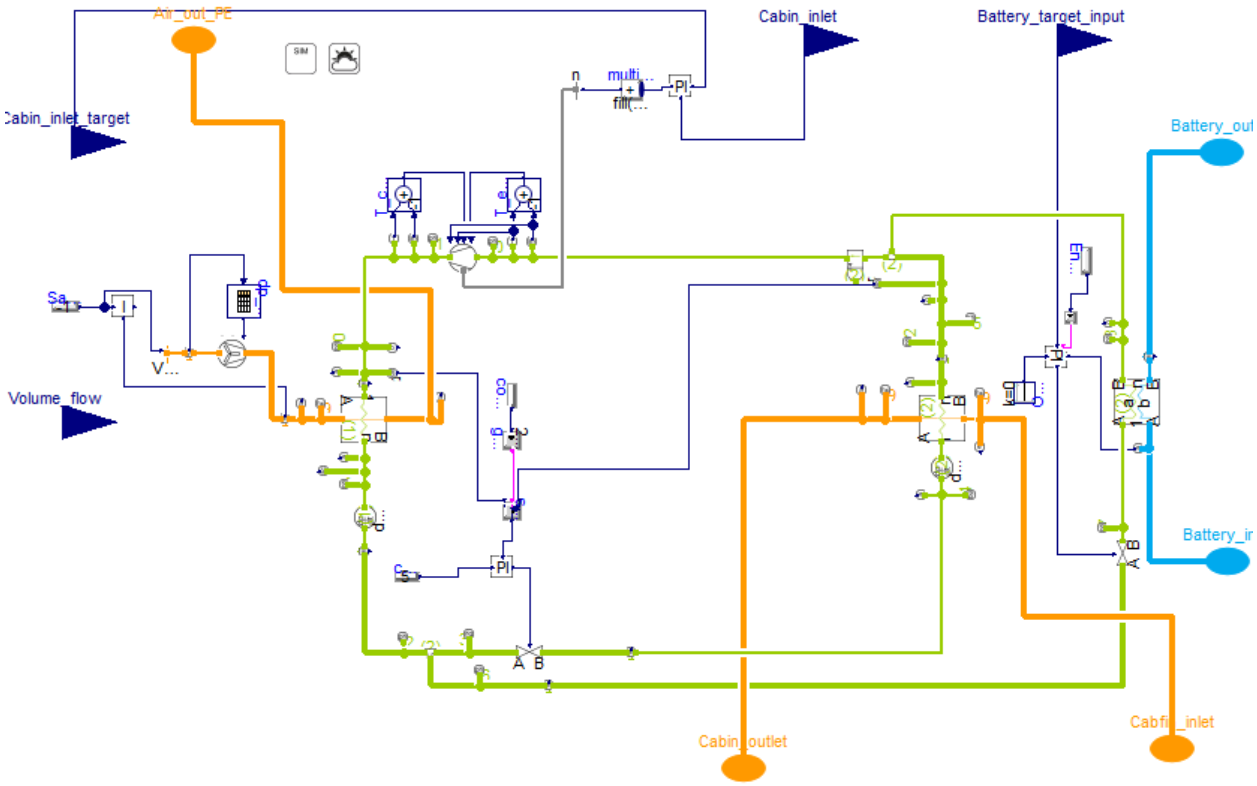

Figure A7: HVAC sub-model in Modelica environment

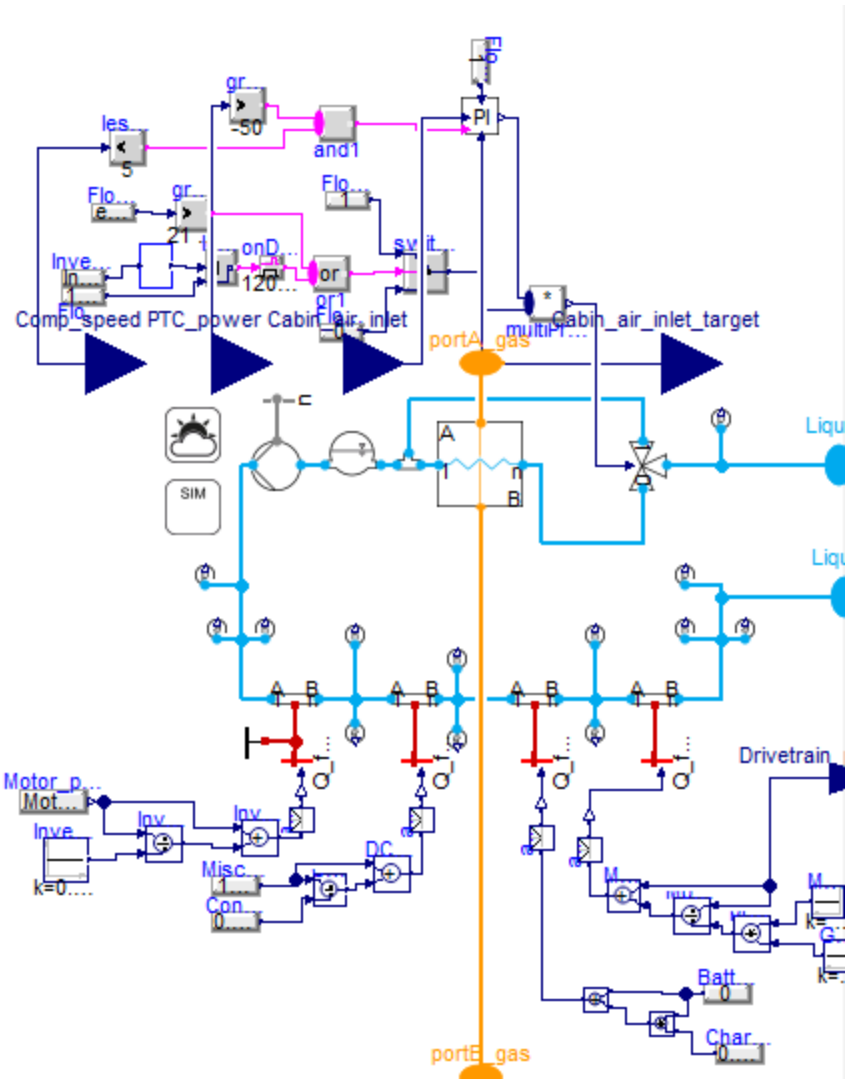

Figure A8: Power electronics sub-model in Modelica environment

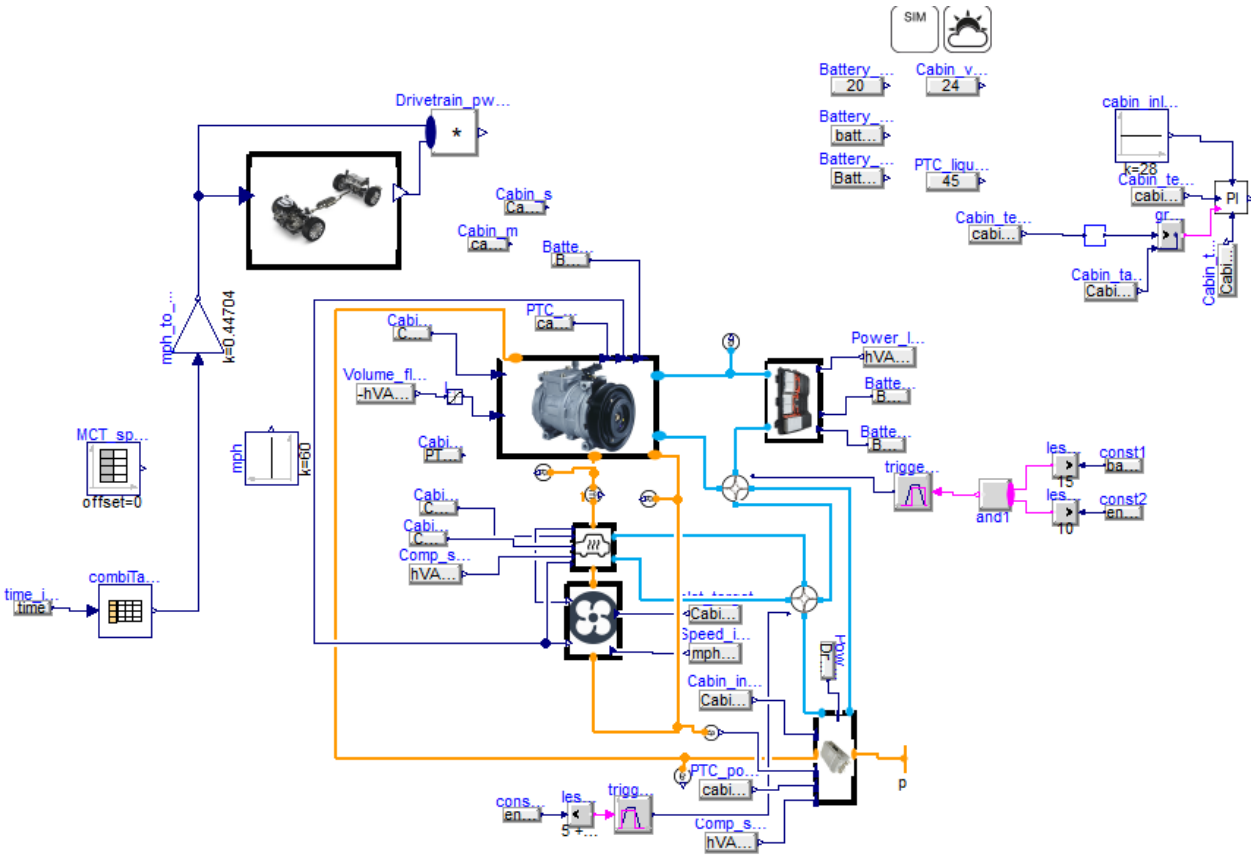

Figure A9: WHR EV model in Modelica environment

REFERNCES

[1] J. Kim, J. Oh and H. Lee, "Review on battery thermal management system for electric vehicles," *Applied Thermal Engineering,* vol. 149, pp. 192-212, 2018.

[2] H. Park, "Numerical assessment of liquid cooling system for power electronics in fuel cell electric vehicles," *International Journal of Heat and Mass Transfer,* vol. 73, pp. 511-520, 2014.

[3] Z. Zhang, J. Wang, X. Feng, L. Chang, Y. Chen and X. Wang, "The solutions to electric vehicle air conditioning systems: A review," *Renewable and Sustainable Energy Reviews*, vol. 91, pp. 443-463, 2018.

[4] B. Yu, J. Yang, D. Wang, J. Shi and J. Chen, "Energy consumption and increased EV range evaluation through heat pump scenarios and low GWP refrigerants in the new test procedure WLTP," *International Journal of Refrigeration*, vol. 100, pp. 2884-294, 2019.

[5] T. Kiss, J. Lustbader and D. Leighton, "Modeling of an Electric Vehicle Thermal Management System in MATLAB/Simulink," *SAE Technical Paper,* no. 2015-01-1708, 2015.

[6] Z. Tian, W. Gan, X. Zhanga, B. Gub and L. Yang, "Investigation on an integrated thermal management system with battery cooling and motor waste heat recovery for electric vehicle," *Applied Thermal Engineering*, vol. 136, pp. 16-27, 2018.

[7] M. Stellato, L. Bergianti and J. Batteh, "Powertrain and thermal system simulation models of a high performance electric road vehicle," in *International Modelica Conference*, Prague, 2017.

[8] J. Meyer, J. Lustbader, N. Agathocleous, A. Vespa, J. Rugh and G. Titov, "Range Extension Opportunities While Heating a Battery Electric Vehicle," *SAE Technical Paper* , no. 2018-01-0066, 2018.

[9] G. De Nunzio, A. Sciarretta, A. Steinerz and A. Mladek, "Thermal management optimization of a heat-pump-based HVAC system for cabin conditioning in electric vehicles," in

Thirteenth International Conference on Ecological Vehicles and Renewable Energies (EVER), Monaco, 2018.

[10] M. Al-Zareer, I. Dincer and M. A. Rosen, "A review of novel thermal management systems for batteries," *International Journal of Energy Research*, vol. 42, no. 10, pp. 3182-3205, 2018.

[11] R. Stadler and A. Maurer, "Methods for Durability Testing and Lifetime Estimation of Thermal Interface Materials in Batteries," *Batteries*, vol. 5, no. 1, p. 34, 2019.

[12] A. Maurer, J. Kalka and A. Wießler, "Smart Design of Electric Vehicle Batteries and Power Electronics Using Thermal Interface Materials," in *EVS30 Symposium*, Stuttgart, 2017.

[13] M. Al-Zareer, I. Dincer and M. Rosen A., "Heat transfer modeling of a novel battery thermal management system," *Numerical Heat Transfer, Part A: Applications*, vol. 73, no. 5, pp. 277-290, 2018.

[14] Y. Huo, Z. Rao, X. Liu and J. Zhao, "Investigation of power battery thermal management by using mini-channel cold plate," *Energy Conversion and Management* , vol. 89, pp. 387-395, 2015.

[15] X. Xu, G. Tong and R. Li, "Numerical study and optimizing on cold plate splitter for lithium battery thermal management system," *Applied Thermal Engineering*, vol. 167, p. 114787, 2020.

[16] A. Tang, J. Li, L. Lou, C. Shan and X. Yuan, "Optimization design and numerical study on water cooling structure for power lithium battery pack," *Applied Thermal Engineering*, vol. 159, p. 113760, 2019.

[17] J. Shen, Y. Wang, G. Yu and H. Li, "Thermal Management of Prismatic Lithium-Ion Battery with Minichannel Cold Plate," *Journal of Energy Engineering*, vol. 146, no. 1, p. 04019033, 2020.

[18] T. Deng, G. Zhang, Y. Ran and P. Liu, "Thermal performance of lithium ion battery pack by using cold plate," *Applied Thermal Engineering*, vol. 160, p. 114088, 2019.

[19] D.-C. Lee, J.-J. Lee, J.-S. Kim, S. Cho and C.-W. Kim, "Thermal behaviors analysis of 55 Ah large-format lithium-ion pouch cells with different cell aspect ratios, tab locations, and C-rates," *Applied Thermal Engineering*, vol. 175, p. 115422, 2020.

[20] G. Titov and J. Lustbader, "Modeling control strategies and range impacts for electric vehicle integrated thermal management systems with MATLAB/Simulink," *SAE Technical Paper*, no. 2017-01-0191, 2017.

[21] A. Carriero, M. Locatelli, K. Ramakrishnan, G. Mastinu and M. Gobbi, "A review of the state of the art of electric traction motors cooling techniques," *SAE Technical Paper*, no. 2018-01-0057, 2018.

[22] K. J. Kelly, T. Abraham, K. Bennion, D. Bharathan, S. Narumanchi and M. O'Keefe, "Assessment of thermal control technologies for cooling electric vehicle power electronics," in *23rd International Electric Vehicle Symposium (EVS-23)*, Anaheim, 2007.

[23] A. Bhunia, S. Chandrasekaran and C.-L. Chen, "Performance improvement of a power conversion module by liquid micro-jet impingement cooling," *IEEE Transactions on Components and Packaging Technologies*, vol. 30, no. 3, pp. 309-316, 2007.

[24] Z. Wang, M. Wei, F. Peng, H. Liu, C. Guo and G. Tian, "Experimental evaluation of an integrated electric vehicle AC/HP system operating with R134a and R407C," *Applied Thermal Engineering*, vol. 100, pp. 1179-1188, 2016.

[25] S. E. Mattsson and H. Elmqvist, "Modelica - An International Effort to Design the Next Generation Modeling Language," *IFAC Proceedings Volumes*, vol. 30, no. 4, pp. 151-155, 1997.

[26] T. J. Shelly, J. A. Weibel, D. Ziviani and E. A. Groll, "A Dynamic Simulation Framework for the Analysis of Battery Electric Vehicle Thermal Management Systems," in *19th IEEE Intersociety Conference on Thermal and Thermomechanical Phenomena in Electronic Systems (ITherm)*, Orlando, 2020.

[27] TLK-Thermo GmbH, "TLK-Thermo – Engineering Services and Software for Thermal Systems," TLK-Thermo GmbH, [Online]. Available: https://www.tlk-thermo.com/index.php/en/. [Accessed 07 1 2020].

[28] K. Olejniczak, T. Flint, D. Simco, S. Storkov, B. McGee, R. Shaw, B. Passmore, K. George, A. Curbow and T. McNutt, "A compact 110 kVA, 140°C ambient, 105°C liquid cooled, all-SiC inverter for electric vehicle traction drives," in *IEEE Applied Power Electronics Conference and Exposition (APEC)*, Tampa, 2017.

[29] L. Fang, M.-S. Kim, J.-Y. Lim and K.-C. Kim, "Study on design and control strategy of interior permanent magnet synchronous motor for high efficiency and wide constant-power operation," in *International Conference on Electrical Machines and Systems*, 2013.

[30] G. Wu, X. Zhang and Z. Dong, "Impacts of two-speed gearbox on electric vehicle's fuel economy and performance," *SAE Technical Paper*, no. 2013-01-0349, 2013.

[31] N. Hasan, M. Anwar, M. Teimorzadeh and D. Tasky, "Features and challenges for auxiliary power module (APM) design for hybrid/electric vehicle applications," in *IEEE Vehicle Power and Propulsion Conference*, Chicago, 2011.

[32] L. Lam, P. Bauer and E. Kelder, "A practical circuit-based model for Li-ion battery cells in electric vehicle applications," in *IEEE 33rd International Telecommunications Energy Conference (INTELEC)*, Amsterdam, 2011.

[33] J. Jaguemont, L. Boulon and Y. Dubé, "Characterization and Modeling of a Hybrid-Electric-Vehicle Lithium-Ion Battery Pack at Low Temperatures," *IEEE Transactions on Vehicular Technology*, vol. 65, no. 1, pp. 1-14, 2015.

[34] Y. Tripathy, A. Mcgordon and C. Low, "A New Consideration for Validating Battery Performance at Low Ambient Temperatures," *Energies*, vol. 11, no. 9, p. 2439, 2018.

[35] T. Huria, M. Ceraolo, J. Gazzarri and R. Jackey, "High fidelity electrical model with thermal dependence for characterization and simulation of high power lithium battery cells," in *IEEE International Electric Vehicle Conference*, Greenville, 2012.

[36] D. Cittanti, A. Ferraris, A. Airale, S. Fiorot, S. Scavuzzo and M. Carello, "Modeling Li-ion batteries for automotive application: A trade-off between accuracy and complexity," in *International Conference of Electrical and Electronic Technologies for Automotive*, Torino, 2017.

[37] S. Arianto, R. Y. Yuwono and B. Prihandoko, "Modeling of Lithium Ion Battery Using Modelica and Scilab/Xcos," in *ECS Transactions*, San Diego, 2016.

[38] A. Nikolian, J. Jaguemont, J. D. Hoog, S. Goutam, N. Omar, P. V. D. Bossche and J. V. Mierlo, "Complete cell-level lithium-ion electrical ECM model for different chemistries (NMC, LFP, LTO) and temperatures (−5 °C to 45 °C) – Optimized modelling techniques," *International Journal of Electrical Power & Energy Systems*, vol. 98, pp. 133-146, 2018.

[39] A. Fotouhi, S. Longo, D. Auger and K. Propp, "Electric Vehicle Battery Parameter Identification and SOC Observability Analysis: NiMH and Li-S Case Studies," in *8th IET International Conference on Power Electronics, Machines and Drives*, Glasgow, 2016.

[40] Y. Chen, Y. Ma, P. Duan and H. Chen, "Estimation of State of Charge for Lithium-ion Battery Considering Effect of Aging and Temperature," in *Chinese Control Conference*, Wuhan, 2018.

[41] Z. Yang, D. Patil and B. Fahimi, "Electrothermal Modeling of Lithium-Ion Batteries for Electric Vehicles," *IEEE Transactions on Vehicular Technology,* vol. 68, no. 1, pp. 170-179, 2019.

[42] M. Bahramipanah, D. Torregrossa, R. Cherkaoui and M. Paolone, "Enhanced Equivalent Electrical Circuit Model of Lithium-Based Batteries Accounting for Charge Redistribution, State-of-Health, and Temperature Effects," *IEEE Transactions on Transportation Electrification,* vol. 3, no. 3, pp. 589-599, 2017.

[43] N. A. Samad, J. B. Siegel and A. G. Stefanopoulou, "Parameterization and Validation of a Distributed Coupled Electro-Thermal Model for Prismatic Cells," in *ASME 2014 Dynamic Systems and Control Conference* , San Antonio, 2015.

[44] M. Yazdanpour, P. Taheri, A. Mansouri and B. Schweitzer, "A circuit-based approach for electro-thermal modeling of lithium-ion batteries," in *32nd Thermal Measurement, Modeling & Management Symposium (SEMI-THERM),* San Jose, 2016.

[45] A. I. Stroe, D. I. Stroe, M. Swierczynski, R. Teodorescu and S. K. Kær, "Lithium-ion battery dynamic model for wide range of operating conditions," in *International Conference on Optimization of Electrical and Electronic Equipment (OPTIM) & 2017 Intl Aegean Conference on Electrical Machines and Power Electronics (ACEMP)*, Brasov, 2017.

[46] K. Li, F. Wei, K. J. Tseng and B.-H. Soong, "A Practical Lithium-Ion Battery Model for State of Energy and Voltage Responses Prediction Incorporating Temperature and Ageing Effects," *IEEE Transactions on Industrial Electronics,* vol. 65, no. 8, pp. 6696-6708, 2018.

[47] V. Gnielinski, "New Equations for Heat and Mass Transfer in Turbulent Pipe and Channel Flow," *International Chemical Engineering,* vol. 16, no. 2, pp. 359-368, 1976.

[48] F. W. Dittus and L. M. Boelter, "“Heat transfer in automobile radiators of the tubular type," *Publications in Engineering,* vol. 2, p. 443, 1930.

[49] Y.-J. Chang and C.-C. Wang, "A generalized heat transfer correlation for louver fin geometry," *International Journal of Heat and Mass Transfer,* vol. 40, no. 3, pp. 533-544, 1997.

[50] S. M. M, "A new correlation for heat transfer during boiling flow through pipes," *ASHRAE Transactions,* vol. 82, pp. 66-86, 1976.

[51] J. C. Chen, "Correlation for Boiling Heat Transfer to Saturated Fluids in Convective Flow," *Industrial & Engineering Chemistry Process Design and Development ,* vol. 5, no. 2, pp. 322-329, 1966.

[52] G. Longo, S. Mancin, G. Righetti and C. Zilio, "A new model for refrigerant boiling inside Brazed Plate Heat Exchangers (BPHEs)," *International Journal of Heat and Mass Transfer*, vol. 91, pp. 144-149, 2015.

[53] S. Haaf, Wärmeübergang in Luftkühlern, Berlin: Springer Verlag, 1988, pp. 435-491.

[54] M. Shah, "A general correlation for heat transfer during film condensation inside pipes," *International Journal of Heat and Mass Transfer,* vol. 22, no. 4, p. 547–556, 1979.

[55] H. &. R. I. Air-Conditioning, "Performance Rating Of Positive Displacement Refrigerant Compressors and Compressor Units," *AHRI Standard,* vol. 540, 2015.

[56] B. Yu, J. Yang, D. Wang, J. Shi and J. Chen, "Energy consumption and increased EV range evaluation through heat pump scenarios and low GWP refrigerants in the new test procedure WLTP," *International Journal of Refrigeration,* vol. 100, pp. 284-294, 2019.

[57] F. Nielsen, S. Gullman, F. Wallin, Å. Uddheim and J.-O. Dalenbäck, "Simulation of Energy Used for Vehicle Interior Climate,," *SAE International Journal of Passenger Cars and Mechancial Systems,* vol. 8, no. 4, pp. 1218-1234, 2015.

[58] SAE, *Surface vehicle reccomended practice: Battery Electric Vehicle Energy Consumption and Range Test Procedure,* 2017.

[59] D.-C. Lee, J.-J. Lee, J.-S. Kim, S. Cho and C.-W. Kim, "Thermal behaviors analysis of 55 Ah large-format lithium-ion pouch cells with different cell aspect ratios, tab locations, and C-rates," *Applied Thermal Engineering,* vol. 175, pp. 115422,, 2020.

[60] J. Cui, J. Wang, J. Weibel and L. Pan, "A compliant microstructured thermal interface material for dry and pluggable interfaces," *Internationl Journal of Heat and Mass Transfer*, vol. 131, pp. 1075-1082, 2019.

VITA

Tyler James Shelly was born on October 1st, 1995 in Newton Kansas and spent the first twenty-three years commuting in and out of Newton for school. Their undergraduate education was completed in 2018 with the completion of a bachelor's in science and mechanical engineering (BSME) and a minor in mathematics. A Dean's list awardee for each semester of undergraduate study, they began graduate school at Purdue University conducting research for the Cooling Technologies Research Center (CTRC). Additionally, they worked on the dynamic modeling, charge optimization, and design of a cold climate heat pump currently planned to be constructed in 2021. They are expected to be awarded a Masters in Science and Mechanical Engineering in December of 2020 from the School of Mechanical Engineering at Purdue University with a focus on thermomechanical design and optimization of electric vehicle thermal management systems. This work included the dynamic and steady state simulation of electric vehicle thermal management systems and battery modules, respectively. Additionally, work and research experience extend into the dynamic modeling and charge optimization of a cold climate heat pump planned to be constructed in 2021. They will continue PhD work at Purdue focusing on EV thermal management systems.